Chaos, Solitons and Fractals 175 (2023) 113932

Contents lists available at ScienceDirect

Chaos, Solitons and Fractals

journal homepage: www.elsevier.com/locate/chaos

On the qualitative study of a discrete fractional order prey–predator model with the effects of harvesting on predator population

Md. Jasim Uddin [a,*], Sarker Md. Sohel Rana [a], Seval Işık [b], Figen Kangalgil [c]

[a] Department of Mathematics, University of Dhaka, Dhaka 1000, Bangladesh
[b] Sivas Cumhuriyet University, Faculty of Education, Department of Mathematics and Science Education, 58140 Sivas, Turkey
[c] Dokuz Eylul University, Bergama Vocational School, 35700 Izmir, Turkey

ARTICLE INFO

MSC:
39A30
39A33
70K50
92D25

Keywords:
Prey-predator model
Caputo fractional derivative
Period-doubling(PD) and Neimark–Sacker (NS) bifurcations
Harvesting
0-1 chaos test
Chaos control

ABSTRACT

This research investigates the discrete prey–predator model by including harvesting on the predator population, in the sense of Caputo fractional derivative. We define the topological categories of the model fixed points. We demonstrate mathematically that, under certain parametric conditions, a fractional order prey-predator model undergoes both a Neimark–Sacker (NS) and a Period-doubling (PD) bifurcations. Using the central manifold and bifurcation theory, we present proof for NS and PD bifurcations. It has been discovered that the fractional order prey-predator model's dynamical behavior is significantly influenced by the parameter values and the initial conditions. Two chaos control techniques have been used to eliminate the chaos in the model. In order to support our theoretical and analytical results and to illustrate complex and chaotic behavior, numerical simulations have been shown.

1. Introduction

Studying the relationship between different ecological phenomena, predator and prey interactions have become very popular in ecological science. The two most prominent types of mathematical frameworks in population dynamics are continuous and discrete-time models. The prey-predator paradigm is a fundamental model in population dynamics that is used to analyze the dynamics of interacting groups [1]. Population dynamics have used continuous-time population models, such as the Lotka–Volterra model [2,3], to understand the interaction between ecological organisms [4,5]. Since it ignores many real-world events and complexity, many researchers have changed this model over time to provide a more realistic explanation and improve comprehension. However, discrete-time population models have also received attention recently [6,7] because they can produce more intricate and fascinating dynamical behaviors than continuous-time models and are more appropriate for modeling populations with non-overlapping generations. For instance, a 1-dimensional discrete-time autonomous system can display chaos, whereas a continuous-time setup necessitates at least a 3-dimensional autonomous system [8].

Each population in an ecological system uses a different strategy, such as refuging, grouping, etc to find food sources and protect itself. To create more realistic mathematical models, a variety of ecological factors and components are used. Every prey-predator encounter must take into account the functional response in population dynamics, which is the quantity of prey consumed by a predator in relation to the density of the prey per unit of time. For the majority of arthropod predators, the functional response of the Holling type II [9] is better than those from the Holling types I, III, and IV. Ivlev [10] developed a new functional response, known as the Ivlev functional response, to investigate the dynamical interaction between prey and predator species:

$$p(x) = \eta(1 - \exp(-ax))y,$$

where the positive constants η and a stand for the greatest rate of predation and the lowest desire to hunt, respectively. There have been numerous studies of predator–prey interaction with Ivlev-type functional reactions. The results have suggested that Ivlev-type relationships between the species have several models in ecological applications, including dynamics in host-parasite models [11], predator–prey models [12], and animal coat patterns [13]. Some authors also used

* Corresponding author.
E-mail addresses: jasimu00@gmail.com (M.J. Uddin), srana.mthdu@gmail.com (S.M.S. Rana), skaracan@cumhuriyet.edu.tr (S. Işık), figen.kangalgil@deu.edu.tr (F. Kangalgil).

https://doi.org/10.1016/j.chaos.2023.113932
Received 10 May 2023; Received in revised form 2 August 2023; Accepted 8 August 2023
Available online 25 August 2023

different functional responses in the prey-predator model [14] and the phytoplankton-zooplankton model [15].

The following mechanism is always present in the traditional predator–prey relationship:

$$\dot{x} = x\tilde{Y}(x,k) - y\tilde{\Theta}(x)$$
$$\dot{y} = y(-\delta + \tilde{\Omega}(x))$$

with

$$x(0), y(0) > 0.$$

where the time-dependent functions $x(t)$ and $y(t)$ stand in for the prey and predator population densities, respectively. Every constant is assumed to be positive. The carrying capacity is indicated by the parameter k. The predator's mortality rate is represented by the constant δ. $\tilde{\Theta}(x)$ represents the functional response, while $\tilde{\Omega}(x)$ represents the uptake functions. The following predator–prey system with logistic growth on prey will be taken into consideration when accounting for the Ivlev functional response [16]:

$$\begin{aligned} \dot{x} &= rx\left(1 - \frac{x}{k}\right) - \eta(1 - e^{-ax})y \\ \dot{y} &= \beta(1 - e^{-ax})y - dy \end{aligned} \tag{1}$$

The prey's growth rate is indicated by the parameter r, and the rate at which the prey becomes a predator after being digested is indicated by the parameter β.

The coexistence of interacting populations depends critically on their dynamical behaviours. Knowing the population density, growth patterns, etc., in particular places is crucial in many situations. Chaos's emergence is extremely detrimental to population expansion. Over generations, it causes complex, erratic variations in population density. Therefore, the management of chaos is crucial for the peaceful cohabitation of communities. Chaos is unusual in populations in the real world, though. Harvesting is the process of removing a subset of a population. It is a characteristic shared by numerous populations. Additionally, it is a popular and simple method for handling naturally occurring chaos. Authors in [17] thoroughly examined several organised structures of two logistic maps that were linearly coupled but had distinct harvesting methods. New organised structures in bi-parameter space for a nonlinear discrete predator–prey model with cooperative hunting are reported by N.C. Pati et al. [18]. Many ecological concepts, such as diffusion, functional responses, the Allee effect, and harvesting have been added to the predator–prey models to facilitate a more accurate description. It is known to all that one of the important modifications to the system is harvesting. Researching the predator–prey phenomena makes it practical to assess the effects of harvesting. Population harvesting [19] is a common practice in the administration of fisheries, forests, and wildlife. Incorporating harvesting on predator population, the above model (1) becomes:

$$\begin{aligned} \dot{x} &= rx\left(1 - \frac{x}{k}\right) - \eta(1 - e^{-ax})y \\ \dot{y} &= \beta(1 - e^{-ax})y - dy - \gamma y \end{aligned} \tag{2}$$

where γ denotes the harvesting effect. This manuscript aims to analyze the complex dynamical behaviors of the discrete fractional-order version of the system (2).

It is known that an extension of traditional differentiation and integration to any extent is fractional calculus. Its widespread use in many disciplines like biology, fluid dynamics, and medicine, among others, piques the interest of researchers. Fractional order calculus has attracted the interest of scholars due to its use in a variety of fields [20,21] over the past 20 years. Many authors have lately investigated biological models [22,23] using fractional order. The main reason is that memory-based systems, which are common in most living systems [24,25], are inextricably linked to fractional order models. Memory effects, or the impact of previous states on the current dynamics, can naturally exist in a variety of prey-predator populations in biological systems. Memory effects are crucial in some instances: migratory prey, predators with learning, delayed growth response, prey with reproduction delays, evolutionary adaptations, prey with hibernation or diapause, predator learning and forgetting and so on. A fractional-order prey-predator model was presented by Javidi et al. [26] and its biological behaviors were explored. Because it functions in the same way as regular derivatives, the prey-predator paradigm is compatible with fractional derivatives. The population's rate of change may be slower as a result, which could lead to a more precise mathematical estimate.

There are various definitions for fractional derivatives. One of the most popular definitions is Caputo's definition of fractional derivatives, which is commonly applied in real-world settings. The Caputo derivative offers a powerful and practical approach for modeling fractional-order predator–prey interactions, ensuring the preservation of equilibrium states, and facilitating the application of standard initial and boundary conditions for accurate and insightful ecological predictions. Its versatility and ability to capture memory effects make it a valuable tool for investigating complex ecological dynamics in various real-world problems [27].

Definition 1. Consider

$$D^{\alpha} f(t) = J^{l-\alpha} f^{(l)}(t), \quad \alpha > 0$$

where f^{l} denotes the derivative of $f(t)$ in the $l-$order, $l = [\alpha]$ is the value of α rounded up to the nearest integer, and J^{q} is the operator for the Riemann–Liouville integral of $q-$ order.

$$J^{q} h(t) = \frac{\int_0^t (t-\tau_e)^{q-1} h(\tau_e) d\tau_e}{\Gamma(q)}, \quad q > 0$$

where $\Gamma(.)$ is the gamma function of Euler. The operator D^{α} is also known as the "$\alpha-$order Caputo differential operator".

Now we apply the Caputo fractional derivatives to the continuous system (2) and provide a theoretical explanation of the bifurcation occurrences:

$$\begin{aligned} D^{\alpha} x(t) &= rx\left(1 - \tfrac{x}{k}\right) - \eta(1 - e^{-ax})y \\ D^{\alpha} y(t) &= \beta(1 - e^{-ax})y - dy - \gamma y \end{aligned} \tag{3}$$

The following are the research's main contributions:

(1) The intended paradigm consists of two interdependent species. We examined how harvesting impacted the model's community of predators and the community of prey.

(2) Potential fixed points are looked after while evaluating the model's stability.

(3) The ability of the suggested model to experience PD and NS bifurcations has been established.

(4) The PD and NS bifurcations have made the model chaotic, so the OGY (Ott, Grebogi, and Yorke) and state feedback control methods have been used to control it.

(5) A few numerical examples have been offered to demonstrate the validity of our theoretical conclusions.

This paper is organized into the following sections: The fractional-order parameterized discretized-time prey-predator model is built in Section 2. In Section 3, the topological classifications of the fixed points are investigated. The possibility of a PD or NS bifurcation of the fractional-order model under a specific parametric condition is mathematically investigated in Section 4. To back our analytical findings, we numerically illustrate model dynamics in Section 5 along with bifurcation diagrams and phase portraits. The chaotic model's chaos is stabilized in Section 6 by using the OGY and state feedback management methods. Section 7 offers a succinct explanation.

2. Discretization process

For the discretization of the system (3), we apply an approximation given in [28]. Consider the model (3) with $x(0) = x_0$ and $y(0) = y_0$ are as the initial conditions. By piecewise constant arguments system (3) can be written as

$$D^{\alpha}x(t) = rx\left(\left[\frac{t}{\rho}\right]\rho\right)\left(1-\frac{x\left(\left[\frac{t}{\rho}\right]\rho\right)}{k}\right)-\eta\left(1-e^{-ax\left(\left[\frac{t}{\rho}\right]\rho\right)}\right)y\left(\left[\frac{t}{\rho}\right]\rho\right)$$
$$D^{\alpha}y(t) = \beta\left(1-e^{-ax\left(\left[\frac{t}{\rho}\right]\rho\right)}\right)y\left(\left[\frac{t}{\rho}\right]\rho\right)-dy\left(\left[\frac{t}{\rho}\right]\rho\right)-\gamma y\left(\left[\frac{t}{\rho}\right]\rho\right) \tag{4}$$

where $[t]$ stands for the number components of $t \in [0,+\infty)$ with $t \geq 0$ and ρ stands for discretization constant.

Let $t \in [0,\rho)$, then $\frac{t}{\rho} \in [0,1)$. Thus, we obtain

$$D^{\alpha}x(t) = rx_0\left(1-\frac{x_0}{k}\right)-\eta\left(1-e^{-ax_0}\right)y_0$$
$$D^{\alpha}y(t) = \beta\left(1-e^{-ax_0}\right)y_0-dy_0-\gamma y_0$$

The answer to (4) is simplified to

$$\begin{aligned} x_1(t) &= x_0 + J^{\alpha}\left(rx_0\left(1-\frac{x_0}{k}\right)-\eta\left(1-e^{-ax_0}\right)y_0\right) \\ &= x_0 + \frac{t^{\alpha}}{\Gamma(\alpha+1)}\left(rx_0\left(1-\frac{x_0}{k}\right)-\eta\left(1-e^{-ax_0}\right)y_0\right) \end{aligned}$$

Similarly,

$$\begin{aligned} y_1(t) &= y_0 + J^{\alpha}\left(\beta\left(1-e^{-ax_0}\right)y_0-dy_0-\gamma y_0\right) \\ &= y_0 + \frac{t^{\alpha}}{\Gamma(\alpha+1)}\left(\beta\left(1-e^{-ax_0}\right)y_0-dy_0-\gamma y_0\right) \end{aligned}.$$

Secondly, let $t \in [\rho,2\rho)$. So, $\frac{t}{\rho} \in [1,2)$. Hence,

$$D^{\alpha}x(t) = rx_1\left(1-\frac{x_1}{k}\right)-\eta\left(1-e^{-ax_1}\right)y_1$$
$$D^{\alpha}y(t) = \beta\left(1-e^{-ax_1}\right)y_1-dy_1-\gamma y_1$$

We get the following solution

$$\begin{aligned} x_2(t) &= x_1(\rho) + J_{\rho}^{\alpha}\left(rx_1(\rho)\left(1-\frac{x_1(\rho)}{k}\right)-\eta\left(1-e^{-ax_1(\rho)}\right)y_1(\rho)\right) \\ &= x_1(\rho) + \frac{(t-\rho)^{\alpha}}{\Gamma(\alpha+1)}\left(rx_1(\rho)\left(1-\frac{x_1(\rho)}{k}\right)-\eta\left(1-e^{-ax_1(\rho)}\right)y_1(\rho)\right) \end{aligned},$$

$$\begin{aligned} y_2(t) &= y_1(\rho) + J_{\rho}^{\alpha}\left(\beta\left(1-e^{-ax_1(\rho)}\right)y_1(\rho)-dy_1(\rho)-\gamma y_1(\rho)\right) \\ &= y_1(\rho) + \frac{(t-\rho)^{\alpha}}{\Gamma(\alpha+1)}\left(\beta\left(1-e^{-ax_1(\rho)}\right)y_1(\rho)-dy_1(\rho)-\gamma y_1(\rho)\right) \end{aligned}$$

where $J_{\rho}^{\alpha} \equiv \frac{1}{\Gamma(\alpha)}\int_{\rho}^{t}(t-\tau_e)^{\alpha-1}d\tau_e, \quad \alpha > 0.$

We can readily see that by performing the discretization process n times.

$$\begin{aligned} x_{n+1}(t) &= x_n(n\rho) + \frac{(t-n\rho)^{\alpha}}{\Gamma(\alpha+1)}\left(rx_n(n\rho)\left(1-\frac{x_n(n\rho)}{k}\right)\right. \\ &\quad \left.-\eta\left(1-e^{-ax_n(n\rho)}\right)y_n(n\rho)\right) \\ y_{n+1}(t) &= y_n(n\rho) + \frac{(t-n\rho)^{\alpha}}{\Gamma(\alpha+1)}\left(\beta\left(1-e^{-ax_n(n\rho)}\right)y_n(n\rho)\right. \\ &\quad \left.-dy_n(n\rho)-\gamma y_n(n\rho)\right) \end{aligned}.$$

where $t \in [n\rho,(n+1)\rho)$. For $t \to (n+1)\rho$, we get

$$\begin{aligned} x_{n+1}((n+1)\rho) &= x_n(n\rho) + \frac{\rho^{\alpha}}{\Gamma(\alpha+1)}\left(rx_n(n\rho)\left(1-\frac{x_n(n\rho)}{k}\right)\right. \\ &\quad \left.-\eta\left(1-e^{-ax_n(n\rho)}\right)y_n(n\rho)\right) \\ y_{n+1}((n+1)\rho) &= y_n(n\rho) + \frac{\rho^{\alpha}}{\Gamma(\alpha+1)}\left(\beta\left(1-e^{-ax_n(n\rho)}\right)y_n(n\rho)\right. \\ &\quad \left.-dy_n(n\rho)-\gamma y_n(n\rho)\right) \end{aligned}$$

The discretized form is then provided here using the Caputo fractional derivative on the system (3):

$$\begin{aligned} x_{n+1} &= x_n + \frac{\rho^{\alpha}}{\Gamma(\alpha+1)}\left(rx_n\left(1-\frac{x_n}{k}\right)-\eta\left(1-e^{-ax_n}\right)y_n\right) \\ y_{n+1} &= y_n + \frac{\rho^{\alpha}}{\Gamma(\alpha+1)}\left(\beta\left(1-e^{-ax_n}\right)y_n-dy_n-\gamma y_n\right) \end{aligned} \tag{5}$$

Remark. If $\alpha \to 1$ in (5), it is discovered that the predator–prey model with harvesting under the Euler discretization. Although the fractional order discrete prey-predator model has several benefits over its classical version, it also has limitations. Due to the fractional order discrete prey-predator model's recent development, there is a dearth of empirical data to verify its precision and application to actual systems. Comparatively to traditional discrete models, fractional-order difference equation analysis and solution is more difficult. In comparison to conventional parameters, the determination of fractional order parameters might be more difficult and unpredictable. Additionally in a discrete prey-predator system, taking a fractional order might result in a number of restrictions and complications. Here are a few of the main restrictions: interpretability, non-standard difference equations, increased computational complexity, lack of historical data, uncertain parameter estimation and so on. Despite these drawbacks, fractional order models can shed light on complex systems that involve non-local interactions and memory effects. Non-integer order derivatives and integrals are the focus of fractional calculus. Complex dynamics can be captured using fractional-order differential equations, which is not possible with integer-order models.

3. Existence conditions and fixed point's stability analysis

3.1. Fixed points and their existence

A quick algebraic calculation reveals that the system (5) has the following three fixed points for any value of the permitted parameters:

(i) The trivial fixed point $E_1(0,0)$. There is no prey and predator exist in the ecology.

(ii) The fixed point of the boundary $E_2(k,0)$. According to biology, when there are no predators, the population of prey achieves its carrying limit k.

(iii) If $d+\gamma < \beta(1-e^{-ak})$, then the unique co-existence fixed point $E_3(x^*,y^*)$ exists, where $x^* = -\frac{1}{a}\ln\left[\frac{-(d-\beta+\gamma)}{\beta}\right], y^* = \frac{r\beta x^*(k-x^*)}{k\eta(d+\gamma)}$.

3.2. Analysis of stability for fixed points

We examine the stability of the system (5) at fixed point $E(x,y)$. The magnitude of the eigenvalues of the jacobian matrix calculated at the fixed point $E(x,y)$, it should be noted, impacts the local stability of that fixed point. The jacobian matrix for the fixed point $E(x,y)$ in the system (5) is given by

$$J(x,y) = \begin{pmatrix} \tilde{j_{11}} & \tilde{j_{12}} \\ \tilde{j_{21}} & \tilde{j_{22}} \end{pmatrix} \tag{6}$$

where

$$j_{\tilde{11}} = 1 + \left(\frac{r(k-2x)}{k} - ae^{-ax}\right)\frac{\rho^\alpha}{\Gamma(\alpha+1)},$$

$$j_{\tilde{12}} = (-1+e^{-ax})\frac{\rho^\alpha}{\Gamma(\alpha+1)},$$

$$j_{\tilde{21}} = a\beta y e^{-ax}\frac{\rho^\alpha}{\Gamma(\alpha+1)},$$

$$j_{\tilde{22}} = 1 + (-d+\beta-\gamma-e^{-ax}\beta)\frac{\rho^\alpha}{\Gamma(\alpha+1)}.$$

The defining equation of the Jacobian matrix is denoted by

$$F(\lambda) := \lambda^2 + \hat{p}(x,y)\lambda + \hat{q}(x,y) = 0 \tag{7}$$

where $\hat{p}(x,y) = -(j_{\tilde{11}} + j_{\tilde{22}})$ and $\hat{q}(x,y) = j_{\tilde{11}}j_{\tilde{22}} - j_{\tilde{12}}j_{\tilde{21}}$. The following stability conditions of fixed points are stated using Jury's criterion. The jacobian matrix at $E_1(0,0)$ can be found as

$$J\left(E_1\right) = \begin{pmatrix} 1 + r\frac{\rho^\alpha}{\Gamma(\alpha+1)} & 0 \\ 0 & 1-(d+\gamma)\frac{\rho^\alpha}{\Gamma(\alpha+1)} \end{pmatrix}$$

The eigenvalues of $J\left(E_1\right)$ are $\lambda_1 = 1+r\frac{\rho^\alpha}{\Gamma(\alpha+1)}$ and $\lambda_2 = 1-(d+\gamma)\frac{\rho^\alpha}{\Gamma(\alpha+1)}$

Lemma 1. *The following topological categorization is valid for the trivial fixed point $E_1(0,0)$:*

(i) source if $\rho > \left(\frac{2}{d+\gamma}\Gamma(1+\alpha)\right)^{\frac{1}{\alpha}}$,

(ii) sink if $\rho < \left(\frac{2}{d+\gamma}\Gamma(1+\alpha)\right)^{\frac{1}{\alpha}}$,

(iii) non-hyperbolic if $\rho = \left(\frac{2}{d+\gamma}\Gamma(1+\alpha)\right)^{\frac{1}{\alpha}}$.

The jacobian matrix at $E_2(k,0)$ can be found as

$$J\left(E_2\right) = \begin{pmatrix} 1 - r\frac{\rho^\alpha}{\Gamma(\alpha+1)} & (-1+e^{-ak})\eta\frac{\rho^\alpha}{\Gamma(\alpha+1)} \\ 0 & 1+\left(-d-\gamma+\beta(1-e^{-ak})\right)\frac{\rho^\alpha}{\Gamma(\alpha+1)} \end{pmatrix}.$$

The eigenvalues of $J\left(E_1\right)$ are $\lambda_1 = 1 - r\frac{\rho^\alpha}{\Gamma(\alpha+1)}$ and $\lambda_2 = 1 + \left(-d-\gamma+\beta(1-e^{-ak})\right)\frac{\rho^\alpha}{\Gamma(\alpha+1)}$.

Lemma 2. *The following topological categorization is valid for the predator-free fixed point $E_2(k,0)$:*

(i) if $d+\gamma > \beta(1-e^{-ak})$ then the fixed point $E_2(k,0)$ is

(i.i) sink if $0 < \rho < min\{\left(\frac{2}{r}\Gamma(1+\alpha)\right)^{\frac{1}{\alpha}}, \left(\frac{2}{d+\gamma-\beta(1-e^{-ak})}\Gamma(1+\alpha)\right)^{\frac{1}{\alpha}}\}$,

(i.ii) source if $\rho > max\{\left(\frac{2}{r}\Gamma(1+\alpha)\right)^{\frac{1}{\alpha}}, \left(\frac{2}{d+\gamma-\beta(1-e^{-ak})}\Gamma(1+\alpha)\right)^{\frac{1}{\alpha}}\}$,

(i.iii) non-hyperbolic if $\rho = \left(\frac{2}{r}\Gamma(1+\alpha)\right)^{\frac{1}{\alpha}}$ *or* $\rho = \left(\frac{2}{d+\gamma-\beta(1-e^{-ak})}\Gamma(1+\alpha)\right)^{\frac{1}{\alpha}}$,

(ii) if $d+\gamma < \beta(1-e^{-ak})$ then the fixed point $E_2(k,0)$ is

(ii.i) source if $\rho > \left(\frac{2}{r}\Gamma(1+\alpha)\right)^{\frac{1}{\alpha}}$,

(ii.ii) saddle if $\rho < \left(\frac{2}{r}\Gamma(1+\alpha)\right)^{\frac{1}{\alpha}}$,

(ii.iii) non-hyperbolic if $\rho = \left(\frac{2}{r}\Gamma(1+\alpha)\right)^{\frac{1}{\alpha}}$,

(iii) if $d+\gamma = \beta(1-e^{-ak})$ then the fixed point $E_2(k,0)$ is non-hyperbolic.

Naturally, one of the eigenvalues of $J\left(E_2\right)$ is -1 and the other is not equal to ± 1 when $\rho = \left(\frac{2}{r}\Gamma(1+\alpha)\right)^{\frac{1}{\alpha}}$ or $\rho = \left(\frac{2}{d+\gamma-\beta(1-e^{-ak})}\Gamma(1+\alpha)\right)^{\frac{1}{\alpha}}$. Therefore, if parameters change in a limited area around $\widehat{FB}^1_{E1}$ or $\widehat{FB}^2_{E1}$, a PD bifurcation may happen.

$$\widehat{FB}^1_{E1} = \Bigg\{(r,a,k,d,\eta,\beta,\gamma,\rho,\alpha) \in (0,+\infty) : \rho = \left(\frac{2}{r}\Gamma(1+\alpha)\right)^{\frac{1}{\alpha}}, \rho \neq \left(\frac{2}{d+\gamma-\beta(1-e^{-ak})}\Gamma(1+\alpha)\right)^{\frac{1}{\alpha}}\Bigg\},$$

or

$$\widehat{FB}^2_{E1} = \Bigg\{(r,a,k,d,\eta,\beta,\gamma,\rho,\alpha) \in (0,+\infty) : \rho = \left(\frac{2}{d+\gamma-\beta(1-e^{-ak})}\Gamma(1+\alpha)\right)^{\frac{1}{\alpha}}, \rho \neq \left(\frac{2}{r}\Gamma(1+\alpha)\right)^{\frac{1}{\alpha}}\Bigg\}.$$

At $E_3(x^*,y^*)$, the characterizing equation looks like this:

$$F_{ee}(\lambda) := \lambda^2 - (2+\tilde{\Delta}\tilde{\mu_e})\lambda + (1+\tilde{\Delta}\tilde{\mu_e} + \tilde{\Omega}\tilde{\mu_e}^2) = 0 \tag{8}$$

where

$$\tilde{\mu_e} = \frac{\rho^\alpha}{\Gamma(\alpha+1)},$$

$$\tilde{\Delta} = -d + r - \frac{2rx^*}{k} + \beta - e^{-ax^*}\beta - \gamma - ae^{-ax^*}y^*\eta$$

$$\tilde{\Omega} = \frac{1}{k}e^{-ax^*}\left(-2rx^*((-1+e^{ax^*})\beta - e^{ax^*}\gamma) + d(e^{ax^*}r(-k+2x^*) + aky^*\eta)\right) + \frac{1}{k}e^{-ax^*}\left(k(r((-1+e^{ax^*})\beta - e^{ax^*}\gamma) + ay^*\gamma\eta)\right)$$

So $F_{ee}(1) = \tilde{\Omega}\tilde{\mu_e}^2 > 0$ and $F_{ee}(-1) = 4 + 2\tilde{\Delta}\tilde{\mu_e} + \tilde{\Omega}\tilde{\mu_e}^2$. We give the following lemma regarding the stability criteria of E_3.

Lemma 3. *The following topological categorization is valid for the co-existence fixed point $E_3(x^*,y^*)$:*

(i) source if

(i.i) $\tilde{\Delta}^2 - 4\tilde{\Omega} \geq 0$ *and* $\tilde{\mu_e} > \frac{-\tilde{\Delta}+\sqrt{\tilde{\Delta}^2-4\tilde{\Omega}}}{\tilde{\Omega}}$

(i.ii) $\tilde{\Delta}^2 - 4\tilde{\Omega} < 0$ *and* $\tilde{\mu_e} > \frac{-\tilde{\Delta}}{\tilde{\Omega}}$

(ii) sink if

(ii.i) $\tilde{\Delta}^2 - 4\tilde{\Omega} \geq 0$ *and* $\tilde{\mu_e} < \frac{-\tilde{\Delta}-\sqrt{\tilde{\Delta}^2-4\tilde{\Omega}}}{\tilde{\Omega}}$

(ii.ii) $\tilde{\Delta}^2 - 4\tilde{\Omega} < 0$ *and* $\tilde{\mu_e} < \frac{-\tilde{\Delta}}{\tilde{\Omega}}$

(iii) non-hyperbolic if

(iii.i) $\tilde{\Delta}^2 - 4\tilde{\Omega} \geq 0$ *and* $\tilde{\mu_e} = \frac{-\tilde{\Delta}\pm\sqrt{\tilde{\Delta}^2-4\tilde{\Omega}}}{\tilde{\Omega}}; \tilde{\mu_e} \neq \frac{-2}{\tilde{\Delta}}, \frac{-4}{\tilde{\Delta}}$

(iii.ii) $\tilde{\Delta}^2 - 4\tilde{\Omega} < 0$ *and* $\tilde{\mu_e} = \frac{-4}{\tilde{\Delta}}$.

(iv) saddle if otherwise

Let,

$$\widehat{FB}^{1,2}_{E3} = \Bigg\{(r,a,k,d,\eta,\beta,\gamma,\rho,\alpha) : \rho = \left(\frac{-\tilde{\Delta} \pm \sqrt{\tilde{\Delta}^2-4\tilde{\Omega}}}{\tilde{\Omega}}\Gamma(1+\alpha)\right)^{\frac{1}{\alpha}} = \rho_\pm, \tilde{\Delta}^2 - 4\tilde{\Omega} \geq 0, \tilde{\mu_e} \neq \frac{-2}{\tilde{\Delta}}, \frac{-4}{\tilde{\Delta}}\Bigg\}.$$

The system (2) at E_3 undergoes a PD bifurcation, when the parameters $(r,a,k,d,\eta,\beta,\gamma,\rho,\alpha)$ fluctuate within a narrow region of $\widehat{FB}_{E^{1,2}_3}$.

Also, let

$$\widehat{NS}_{E_3} = \left\{(r,a,k,d,\eta,\beta,\gamma,\rho,\alpha) : \rho = \left(\Gamma(1+\alpha)\frac{-\tilde{\Delta}}{\tilde{\Omega}}\right)^{\frac{1}{\alpha}} = \rho_{NS}, \tilde{\Delta}^2 - 4\tilde{\Omega} < 0\right\}.$$

If the parameters $(r,a,k,d,\eta,\beta,\gamma,\rho,\alpha)$ vary around the set $\widehat{NS}_{E_3}$, system (2) will suffer an NS bifurcation at that point.

The model(5)'s positive fixed point's topological categorization for $r = 2.25$, $k = 3.5$, $\beta = 1.05$, $d = 0.1$, $\alpha = 0.75$, $\eta = 0.5$, and with $a \in [0.1, 0.96]$, $\gamma \in [0.25, 0.85]$ and $\rho \in [0.1, 1.5]$ is depicted in Fig. 1(a). The 2D projection is displayed in Fig. 1(b) for $\gamma = 0.5$. Fig. 11 shows the highest Lyapunov exponents and the bifurcation diagram in 2D parametric space.

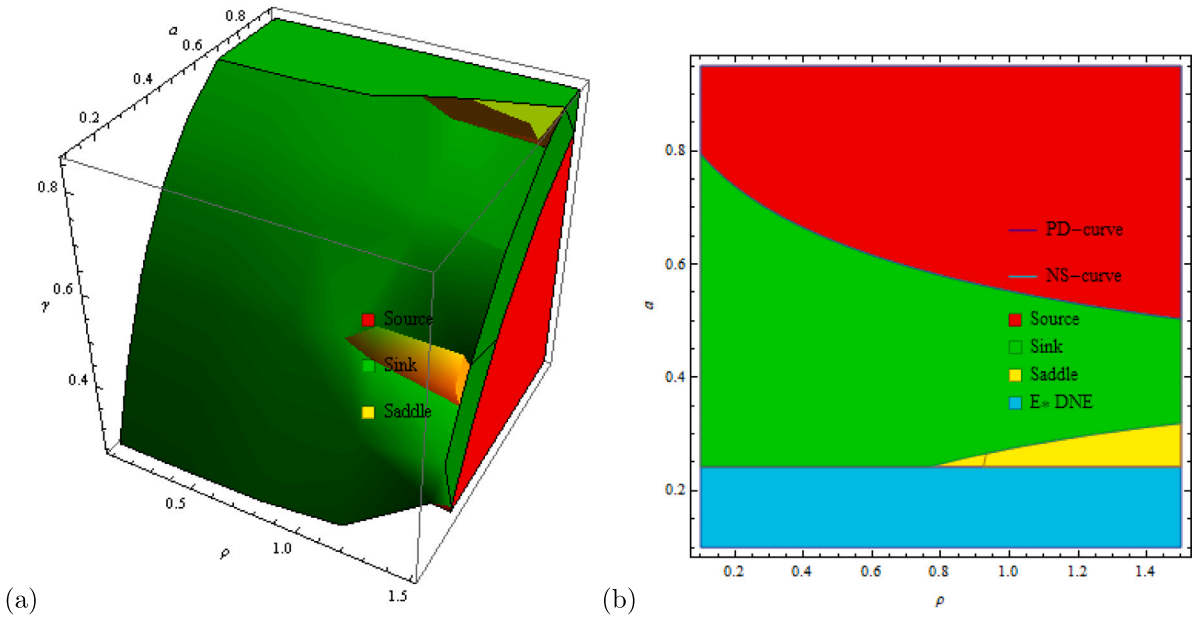

Fig. 1. (a)3D topological categorization of the model(5)'s positive fixed point (b) Stability region (2D) of positive fixed point of the model (5).

4. Analysis of bifurcation

This section introduces a study that will look at the NS and PD bifurcations at the fixed point $E_3(x^*, y^*)$ of the model by using the parameter ρ as a bifurcation parameter.

4.1. Neimark-Sacker bifurcation

The Neimark-Sacker bifurcation surrounding the system (5)'s only positive stable state is examined in this subsection. We have used the traditional theory of bifurcation for the direction and presence of this form of bifurcation. The Neimark-Sacker bifurcation related to various discrete-time mathematical systems [7,29] has lately received attention from a number of mathematicians. For the analysis of NS bifurcation for the positive co-existence fixed point $E_3(x^*, y^*)$, we consider the following study. Assume ρ^* is the small perturbation of ρ where $|\rho^*| \lll 1$. Therefore, the model becomes using perturbation

$$\begin{aligned} x_{n+1} &= x_n + \frac{(\rho+\rho^*)^\alpha}{\Gamma(\alpha+1)}\left(rx_n\left(1-\frac{x_n}{k}\right) - \eta(1-e^{-ax_n})y_n\right) \equiv f(x_n, y_n, \rho^*) \quad (9)\\ y_{n+1} &= y_n + \frac{(\rho+\rho^*)^\alpha}{\Gamma(\alpha+1)}\left(\beta(1-e^{-ax_n})y_n - dy_n - \gamma y_n\right) \equiv g(x_n, y_n, \rho^*) \end{aligned}$$

If $u_n = x_n - x^*, v_n = y_n - y^*$, then equilibrium is $E_3(x^*, y^*)$ becomes the origin, and by using Taylor series at $(u_n, v_n) = (0, 0)$ expanding f and g to the third order, the model (9) becomes

$$\begin{aligned} u_{n+1} =& \alpha_{x1}u_n + \alpha_{x2}v_n + \alpha_{x11}u_n^2 + \alpha_{x12}u_nv_n + \alpha_{x22}v_n^2 + \alpha_{x111}u_n^3 + \alpha_{x112}u_n^2v_n + \\ & \alpha_{x122}u_nv_n^2 + \alpha_{x222}v_n^3 + O((|u_n| + |v_n|)^4) \quad (10)\\ v_{n+1} =& \beta_{y1}u_n + \beta_{y2}v_n + \beta_{y11}u_n^2 + \beta_{y12}u_nv_n + \beta_{y22}v_n^2 + \beta_{y111}u_n^3 + \beta_{y112}u_n^2v_n + \\ & \beta_{y122}u_nv_n^2 + \beta_{y222}v_n^3 + O((|u_n| + |v_n|)^4) \end{aligned}$$

where

$$\begin{aligned} \alpha_{x1} &= 1 + r\left(1 - \frac{2x^*}{k} + \frac{ae^{-ax^*}x^*(-k+x^*)\beta}{k(d+\gamma)}\right)\frac{\rho^\alpha}{\Gamma(\alpha+1)},\\ \alpha_{x2} &= \left(-1+e^{-ax^*}\right)\eta\frac{\rho^\alpha}{\Gamma(\alpha+1)},\\ \alpha_{x11} &= \frac{r\left(-2 + \frac{a^2e^{-ax^*}(k-x^*)x^*\beta}{\gamma+d}\right)\frac{\rho^\alpha}{\Gamma(\alpha+1)}}{k},\\ \alpha_{x12} &= -ae^{-ax^*}\eta\frac{\rho^\alpha}{\Gamma(\alpha+1)},\\ \alpha_{x22} &= 0,\\ \alpha_{x111} &= \frac{a^3e^{-ax^*}(rx^{*2} - krx^*)\beta\frac{\rho^\alpha}{\Gamma(\alpha+1)}}{k(\gamma+d)},\\ \alpha_{x112} &= a^2e^{-ax^*}\eta\frac{\rho^\alpha}{\Gamma(\alpha+1)},\\ \alpha_{x122} &= 0,\\ \alpha_{x222} &= 0,\\ \beta_{y1} &= \frac{ae^{-ax^*}(-rx^{*2} + krx^*)\beta^2\frac{\rho^\alpha}{\Gamma(\alpha+1)}}{k(\gamma+d)\eta},\\ \beta_{y2} &= 1 + \left(\beta - e^{-ax^*}\beta - \gamma - d\right)\frac{\rho^\alpha}{\Gamma(\alpha+1)},\\ \beta_{y11} &= \frac{a^2e^{-ax^*}(rx^{*2} - krx^*)\beta^2\frac{\rho^\alpha}{\Gamma(\alpha+1)}}{k(\gamma+d)\eta},\\ \beta_{y12} &= ae^{-ax^*}\beta\frac{\rho^\alpha}{\Gamma(\alpha+1)},\\ \beta_{y22} &= 0,\\ \beta_{y111} &= \frac{a^3e^{-ax^*}(-rx^{*2} + krx^*)\beta^2\frac{\rho^\alpha}{\Gamma(\alpha+1)}}{k(\gamma+d)\eta},\\ \beta_{y112} &= -a^2e^{-ax^*}\beta\frac{\rho^\alpha}{\Gamma(\alpha+1)},\\ \beta_{y122} &= 0,\\ \beta_{y222} &= 0. \end{aligned} \quad (11)$$

The characteristic equation of the model (10) is $\lambda^2 + p(\rho^*)\lambda + q(\rho^*) = 0$, where $p(\rho^*) = (2 + \tilde{\Delta}\tilde{\mu_e})$ and $q(\rho^*) = (1 + \tilde{\Delta}\tilde{\mu_e} + \tilde{\Omega}\tilde{\mu_e}^2)$, with $\tilde{\mu_e} = \frac{(\rho+\rho^*)^\alpha}{\Gamma(\alpha+1)}$.

The characteristic equation's roots are $\lambda_{1,2}(\rho^*) = \frac{-p(\rho^*) \pm i\sqrt{4q(\rho^*) - (p(\rho^*))^2}}{2}$. From $|\lambda_{1,2}(\rho^*)| = 1$, and $\rho^* = 0$, we have $|\lambda_{1,2}(\rho^*)| = [q(\rho^*)]^{\frac{1}{2}}$ and $l = \left[\frac{d|\lambda_{1,2}(\rho^*)|}{d\rho^*}\right]_{\rho^*=0} \neq 0$. Furthermore, it is imperative that when $\rho^* = 0$, $\lambda_{1,2}^i \neq 1$, $i = 1, 2, 3, 4$, which is equivalent to $p(0) \neq \pm 2, 0, 1$.

To study the normal form, let $\phi = Im(\lambda_{1,2})$ and $\varphi = Re(\lambda_{1,2})$. We ascertain $T = \begin{bmatrix} 0 & 1 \\ \phi & \varphi \end{bmatrix}$, and serving the transformation $\begin{bmatrix} u_n \\ v_n \end{bmatrix} =$

$T\begin{bmatrix}\overline{x}_n\\ \overline{y}_n\end{bmatrix}$, the model (10) becomes

$$\begin{aligned}\overline{x}_{n+1} &= \varphi\overline{x}_n - \phi\overline{y}_n + f_{x11}(\overline{x}_n,\overline{y}_n)\\ \overline{y}_{n+1} &= \phi\overline{x}_n + \varphi\overline{y}_n + g_{y11}(\overline{x}_n,\overline{y}_n),\end{aligned} \tag{12}$$

where the variables $(\overline{x}_n,\overline{y}_n)$ with a rank of at least two are represented by the functions f_{x11} and g_{y11}, respectively, which denote the terms in the model (12).

To transit through NSB, the following discriminating amount Ω must be nonzero: $\Omega = -Re\left[\frac{(1-2\overline{\lambda})\overline{\lambda}^2}{1-\lambda}\xi_{11}\xi_{20}\right] - \frac{1}{2}|\xi_{11}|^2 - |\xi_{02}|^2 + Re(\overline{\lambda}\xi_{21})$, where

$$\begin{aligned}\xi_{20} &= \frac{\varphi}{8}\left(2\beta_{y22} - \varphi\alpha_{x22} - \alpha_{x12} + 4\phi\alpha_{x22} + i\left(4\phi\alpha_{x22} - 2\alpha_{x22} - 2\varphi\alpha_{x22}\right)\right)\\ &\quad + \frac{\phi}{4}\alpha_{x12} + i\frac{1}{8}\left(4\phi\beta_{y22} + 2\phi^2\alpha_{x22} - 2\alpha_{x11}\right) + \frac{\beta_{y12}}{8}\\ &\quad + \frac{\varphi\alpha_{x11} - 2\beta_{y11} + \varphi^3\alpha_{x22} - \varphi^2\beta_{y22} - \varphi^2\alpha_{x12} + \varphi\beta_{y12}}{4\phi},\\ \xi_{11} &= \frac{\phi}{2}(\beta_{y22} - \varphi\alpha_{x22}) + i\frac{1}{2}(\phi^2\alpha_{x22} + \alpha_{y11} + \varphi\alpha_{x12} + \varphi^2\alpha_{x22})\\ &\quad + \frac{\beta_{y11} - \varphi\alpha_{x11} + \varphi\beta_{y12} - \varphi^2\alpha_{x12} - 2\varphi^2\beta_{y22} + 2\varphi^3\alpha_{x22}}{2\phi},\\ \xi_{02} &= \frac{1}{4}\phi(2\varphi\alpha_{x22} + \alpha_{y12} + \beta_{y22}) + i\frac{1}{4}(\beta_{y12} + 2\varphi\beta_{y22} - 2\varphi\alpha_{x12} - \alpha_{x11})\\ &\quad - \frac{\beta_{y11} - \varphi\alpha_{x11} + \varphi\beta_{y12} - \varphi^2\alpha_{x12} + \varphi^2\beta_{y22} - \varphi^3\alpha_{x22}}{4\phi}\\ &\quad + \frac{1}{4}\alpha_{x22}i(\phi^2 - 3\varphi^2),\\ \xi_{21} &= \frac{3}{8}\beta_{y222}(\phi^2 + \varphi^2) + \frac{\beta_{y112}}{8} + \frac{\varphi}{4}\alpha_{x112} + \frac{\varphi}{4}\beta_{y122} + \alpha_{x122}\left(\frac{\phi^2}{8} + \frac{3\varphi^2}{8} - \frac{\varphi}{4}\right)\\ &\quad + \frac{3}{8}\alpha_{x111} + i\frac{3}{8}\alpha_{x222}(\phi^2 + 2\varphi^2) + i\frac{3\phi\varphi}{8}\alpha_{x122}\\ &\quad - \frac{1}{8}\beta_{y122}\phi i - i\frac{3\phi\varphi}{8}\beta_{y222} - i\frac{3\beta_{y111} - 3\varphi\alpha_{x111}}{8\phi}\\ &\quad - i\frac{3\varphi\beta_{y112} - 3\varphi^2\alpha_{x112}}{8\phi} - i\frac{3\varphi^2\beta_{y122} - 3\varphi^3\alpha_{x122}}{8\phi}\\ &\quad - i\frac{3\varphi^3\beta_{y222} - 3\varphi^4\alpha_{x222}}{8\phi}.\end{aligned}$$

We came to the following conclusion as a result of the analysis indicated above.

Theorem 1. }} *If $\Omega \neq 0$, the model proceeds through NS bifurcation at $E_3(x^*,y^*)$ for the parameter ρ to vary in the vicinity of $\widehat{NS}_{E_3}$. If $\Omega < 0$ ($\Omega > 0$), therefore, a smooth closed invariant curve with a positive fixed point $E_3(x^*,y^*)$ can bifurcate and the bifurcation is sub-critical (resp. super-critical).*ε

4.2. Period-doubling bifurcation

This subsection focuses on the possibility of a period-doubling bifurcation at the system (5)'s positive equilibrium point. The center manifold theorem is used to analyze it after normal forms are used to demonstrate the existence and direction of this kind of bifurcation. Numerous experts have recently conducted studies on period-doubling bifurcation in discrete-time mathematical models [15]. The positive fixed point $E_3(x^*,y^*)$'s one eigenvalue is $\lambda_1 = -1$, and the other one is λ_2 neither 1 nor −1, if the systems' parameters vary around the set $\widehat{FB}^{\Gamma,2}_{E3}$. The PD bifurcation is examined using the parameter ρ. Further ρ^* ($|\rho^*| \lll 1$,) is this model perturbation caused by the fluctuations of ρ.

$$\begin{aligned}x_{n+1} &= x_n + \frac{(\rho+\rho^*)^\alpha}{\Gamma(\alpha+1)}\left(rx_n\left(1-\frac{x_n}{k}\right) - \eta(1-e^{-ax_n})y_n\right) \equiv f(x_n,y_n,\rho^*)\\ y_{n+1} &= y_n + \frac{(\rho+\rho^*)^\alpha}{\Gamma(\alpha+1)}\left(\eta(1-e^{-ax_n})y_n - dy_n - \gamma y_n\right) \equiv g(x_n,y_n,\rho^*)\end{aligned} \tag{13}$$

If $u_n = x_n - x^*$, $v_n = y_n - y^*$, then equilibrium $E_3(x^*,y^*)$ becomes the origin, and by using Taylor series about $(u_n,v_n) = (0,0)$ expanding to the third order of f and g, the model (13) becomes

$$\begin{aligned}u_{n+1} =& \alpha_{x1}u_n + \alpha_{x2}v_n + \alpha_{x11}u_n^2 + \alpha_{x12}u_nv_n + \alpha_{x13}u_n\rho^* + \alpha_{x23}v_n\rho^* + \alpha_{x111}u_n^3 +\\ & \alpha_{x112}u_n^2v_n + \alpha_{x113}u_n^2\rho^* + \alpha_{x123}u_nv_n\rho^* + O((|u_n| + |v_n| + |\rho^*|)^4)\\ v_{n+1} =& \beta_{y1}u_n + \beta_{y2}v_n + \beta_{y11}u_n^2 + \beta_{y12}u_nv_n + \beta_{y22}v_n^2 + \beta_{y13}u_n\rho^* + \beta_{y23}v_n\rho^* + \beta_{y111}u_n^3 +\\ & \beta_{y112}u_n^2v_n + \beta_{y113}u_n^2\rho^* + \beta_{y123}u_nv_n\rho^* + \beta_{y223}v_n^2\rho^* + O((|u_n| + |v_n| + |\rho^*|)^4),\end{aligned} \tag{14}$$

where

$$\begin{aligned}\alpha_{x13} &= r\left(1 - \frac{2x^*}{k} + \frac{ae^{-ax^*}x^*(-k+x^*)\beta}{k(d+\gamma)}\right)\frac{\alpha\rho^{\alpha-1}}{\Gamma(\alpha+1)},\\ \alpha_{x23} &= -(1-e^{-ax^*})\frac{\alpha\rho^{\alpha-1}}{\Gamma(\alpha+1)},\\ \alpha_{x113} &= \frac{r}{k}\left(-2 + \frac{a^2e^{-ax^*}x^*(k-x^*)\beta}{(d+\gamma)}\right)\frac{\alpha\rho^{\alpha-1}}{\Gamma(\alpha+1)},\\ \alpha_{x123} &= -ae^{-ax^*}\eta\frac{\alpha\rho^{\alpha-1}}{\Gamma(\alpha+1)},\\ \beta_{y13} &= \frac{ae^{-ax^*}rx^*(k-x^*)\beta^2}{k(d+\gamma)\eta}\frac{\alpha\rho^{\alpha-1}}{\Gamma(\alpha+1)},\\ \beta_{y23} &= \left(-d+\beta-e^{-ax^*}\beta-\gamma\right)\frac{\alpha\rho^{\alpha-1}}{\Gamma(\alpha+1)},\\ \beta_{y113} &= \frac{a^2e^{-ax^*}rx^*(-k+x^*)\beta^2}{k(d+\gamma)}\frac{\alpha\rho^{\alpha-1}}{\Gamma(\alpha+1)},\\ \beta_{y123} &= ae^{-ax^*}\beta\frac{\alpha\rho^{\alpha-1}}{\Gamma(\alpha+1)},\\ \beta_{y223} &= 0.\end{aligned} \tag{15}$$

We assume $T = \begin{bmatrix}\alpha_{x2} & \alpha_{x2}\\ -1-\alpha_{x1} & \lambda_2-\alpha_{x1}\end{bmatrix}$ which is invertible. Now, using the transformation $\begin{bmatrix}u_n\\ v_n\end{bmatrix} = T\begin{bmatrix}\overline{x}_n\\ \overline{y}_n\end{bmatrix}$, the model (14) becomes

$$\begin{aligned}\overline{x}_{n+1} &= -\overline{x}_n + f_{x11}(u_n,v_n,\rho^*)\\ \overline{y}_{n+1} &= \lambda_2\overline{y}_n + g_{y11}(u_n,v_n,\rho^*),\end{aligned} \tag{16}$$

where the variables $(\overline{x}_n,\overline{y}_n)$ with a rank of at least two are represented by the functions f_{x11} and g_{y11}, respectively, which denote the terms in the model (16).

The system (16) has a center manifold $W^c(0,0,0)$ at $(0,0)$ in a highly closed neighborhood of $\rho^* = 0$, which can be deduced using the center manifold theorem and is essentially expressed as follows. $W^c(0,0,0) = \left\{(\overline{x}_n,\overline{y}_n,\rho^*)\,\epsilon R^3 : \overline{y}_{n+1} = \overline{\alpha}_{x1}\overline{x}_n^2 + \overline{\alpha}_{x2}\overline{x}_n\rho^* + O((|\overline{x}_n| + |\rho^*|)^3)\right\}$ where

$$\begin{aligned}\overline{\alpha}_{x1} &= \frac{\alpha_{x2}[(1+\alpha_{x1})\alpha_{x11} + \alpha_{x2}\beta_{y11}]}{1-\lambda_2^2} + \frac{\beta_{y22}(1+\alpha_{x1})^2}{1-\lambda_2^2}\\ &\quad - \frac{(1+\alpha_{x1})[\alpha_{x12}(1+\alpha_{x1}) + \alpha_{x2}\beta_{y12}]}{1-\lambda_2^2},\\ \overline{\alpha}_{x2} &= \frac{(1+\alpha_{x1})[\alpha_{x23}(1+\alpha_{x1}) + \alpha_{x2}\beta_{y23}]}{\alpha_{x2}(1+\lambda_2)^2} - \frac{(1+\alpha_{x1})[\alpha_{x13} + \alpha_{x2}\beta_{y13}]}{(1+\lambda_2)^2}.\end{aligned}$$

The model(16)'s restrained center manifold, $W^c(0,0,0)$, has the following form: $\overline{x}_{n+1} = -\overline{x}_n + h_1\overline{x}_n^2 + h_2\overline{x}_n\rho^* + h_3\overline{x}_n^2\rho^* + h_4\overline{x}_n\rho^{*2} + h_5\overline{x}_n^3 +$

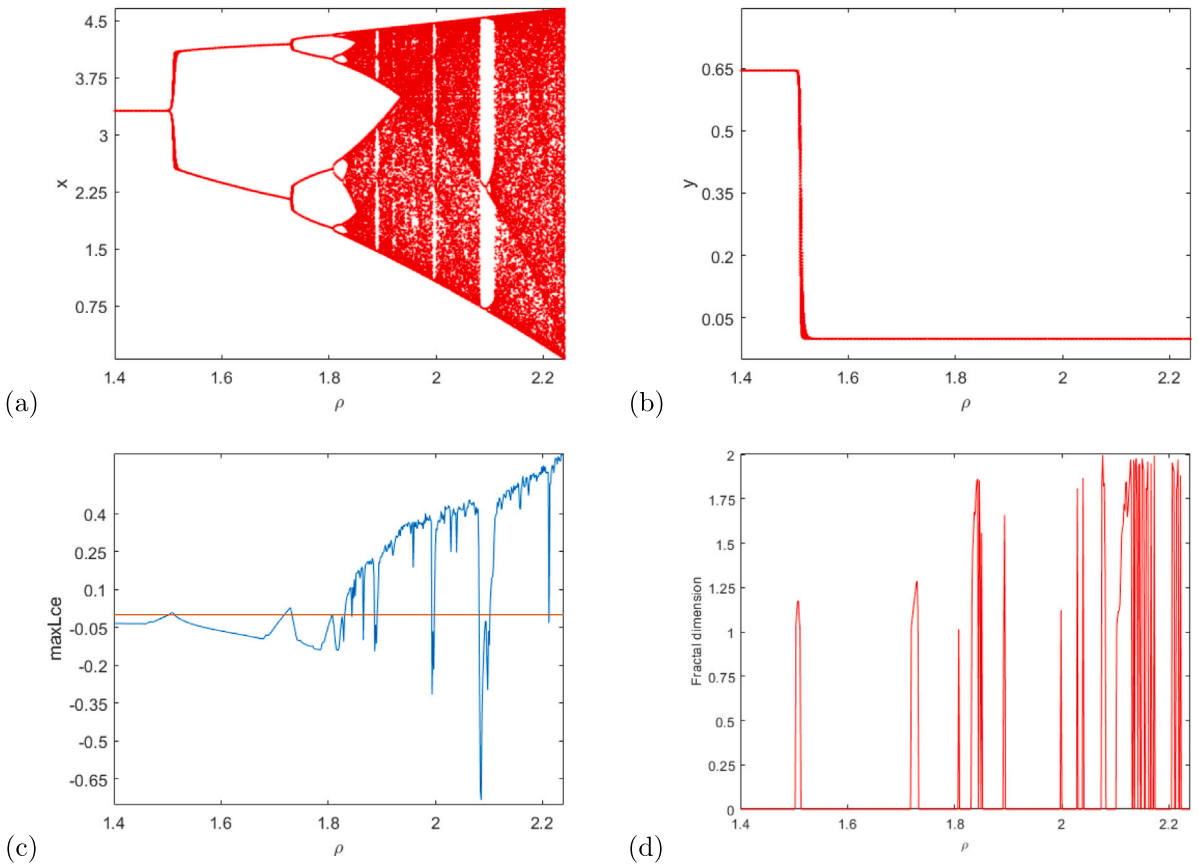

Fig. 2. PD Bifurcation diagram, MLEs and FDs for varying parameter ρ.

$O((|\overline{x}_n| + |\rho^*|)^3) \equiv F(\overline{x}_n, \rho^*)$ where

$$h_1 = \frac{\overline{\alpha}_{x2}[(\lambda_2 - \overline{\alpha}_{x1})\alpha_{x11} - \overline{\alpha}_{x2}\beta_{y11}]}{1+\lambda_2} - \frac{\beta_{x22}(1+\overline{\alpha}_{x1})^2}{1+\lambda_2} - \frac{(1+\overline{\alpha}_{x1})[(\lambda_2 - \overline{\alpha}_{x1})\alpha_{x12} - \overline{\alpha}_{x2}\beta_{y12}]}{1+\lambda_2},$$

$$h_2 = \frac{(\lambda_2 - \overline{\alpha}_{x1})\alpha_{x13} - \overline{\alpha}_{x2}\beta_{y13}}{1+\lambda_2} - \frac{(1+\overline{\alpha}_{x1})[(\lambda_2 - \overline{\alpha}_{x1})\alpha_{x23} - \overline{\alpha}_{x2}\beta_{y23}]}{\overline{\alpha}_{x2}(1+\lambda_2)},$$

$$h_3 = \frac{(\lambda_2 - \alpha_{x1})\overline{\alpha}_{x1}\alpha_{x13} - \alpha_{x2}\beta_{y13}}{1+\lambda_2} + \frac{[(\lambda_2 - \alpha_{x1})\alpha_{x23} - \alpha_{x2}\beta_{y23}](\lambda_2 - \alpha_{x1})\overline{\alpha}_{x1}}{\alpha_{x2}(1+\lambda_2)} - \frac{(1+\alpha_{x1})[(\lambda_2 - \alpha_{x1})\alpha_{x123} - \alpha_{x2}\beta_{y123}]}{1+\lambda_2} + \frac{\alpha_{x2}[(\lambda_2 - \alpha_{x1})\alpha_{x113} - \alpha_{x2}\beta_{y113}]}{1+\lambda_2} - \frac{\beta_{y223}(1+\alpha_{x1})^2}{1+\lambda_2} + \frac{2\alpha_{x2}\overline{\alpha}_{x2}[(\lambda_2 - \alpha_{x1})\alpha_{x11} - \alpha_{x2}\beta_{y11}]}{1+\lambda_2} - \frac{2\beta_{y22}\overline{\alpha}_{x2}(1+\alpha_{x1})(\lambda_2 - \alpha_{x1})}{1+\lambda_2} + \frac{\overline{\alpha}_{x2}[(\lambda_2 - \alpha_{x1})\alpha_{x12} - \alpha_{x2}\beta_{y12}](\lambda_2 - 1 - 2\alpha_{x1})}{1+\lambda_2},$$

$$h_4 = \frac{\overline{\alpha}_{x2}[(\lambda_2 - \alpha_{x1})\alpha_{x13} - \alpha_{x2}\beta_{y13}]}{1+\lambda_2} + \frac{[(\lambda_2 - \alpha_{x1})\alpha_{x23} - \alpha_2\beta_{x23}](\lambda_2 - \alpha_{x1})\overline{\alpha}_{x2}}{\alpha_{x2}(1+\lambda_2)} + \frac{2\alpha_{x2}\overline{\alpha}_{x2}[(\lambda_2 - \alpha_{x1})\alpha_{x11} - \alpha_{x2}\beta_{y11}]}{1+\lambda_2} + \frac{2\beta_{y22}\overline{\alpha}_{x2}(1+\alpha_{x1})(\lambda_2 - \alpha_{x1})}{1+\lambda_2} + \frac{\overline{\alpha}_{x2}[(\lambda_2 - \alpha_{x1})\alpha_{x12} - \alpha_{x2}\beta_{y12}](\lambda_2 - 1 - 2\alpha_{x1})}{1+\lambda_2},$$

$$h_5 = \frac{2\alpha_{x2}\overline{\alpha}_{x1}[(\lambda_2 - \alpha_{x1})\alpha_{x11} - \alpha_{x2}\beta_{y11}]}{1+\lambda_2} + \frac{[(\lambda_2 - \alpha_{x1})\alpha_{x11} - \alpha_{x2}\beta_{y11}](\lambda_2 - 1 - 2\alpha_{x1})\overline{\alpha}_{x1}}{1+\lambda_2} + \frac{2\beta_{y22}\overline{\alpha}_{x1}(\lambda_2 - \alpha_{x1})(1+\alpha_{x1})}{1+\lambda_2} + \frac{\overline{\alpha}_{x2}^2[(\lambda_2 - \alpha_{x1})\alpha_{x111} - \alpha_{x2}\beta_{y111}]}{1+\lambda_2} - \frac{\overline{\alpha}_{x2}(1+\alpha_{x1})[(\lambda_2 - \alpha_{x1})\alpha_{x112} - \alpha_{x2}\beta_{y112}]}{1+\lambda_2}.$$

In order for PD bifurcation to occur, the two differentiating quantities ξ_1 and ξ_2 must both be nonzero, $\xi_1 = \left(\frac{\partial^2 F}{\partial \overline{x}\partial\rho^*} + \frac{1}{2}\frac{\partial F}{\partial \rho^*}\frac{\partial^2 F}{\partial \overline{x}^2}\right)|_{(0,0)}$ and $\xi_2 = \left(\frac{1}{6}\frac{\partial^3 F}{\partial \overline{x}^3} + \left(\frac{1}{2}\frac{\partial^2 F}{\partial \overline{x}^2}\right)^2\right)|_{(0,0)}$.

Finally, the outcome of the analysis above is as follows.

Theorem 2. *"The model experiences PD bifurcation at $E_3(x^*, y^*)$ for varying amounts of ρ in a limited neighborhood of $\widehat{FB}_{E3}^{1,2}$ if $\xi_1 \neq 0$ and $\xi_2 \neq 0$. Further, for $\xi_2 > 0$ ($\xi_2 < 0$) the period-two orbits that bifurcate from $E_3(x^*, y^*)$ is stable (unstable)".*

5. Numerical simulation

We illustrate some novel and intriguing complex dynamical behaviors in the discussed system (5) in this section, and we also provide the system(5)'s bifurcation diagrams, phase portraits, and Lyapunov exponents to support the earlier analytical results. Maximum Lyapunov exponents, known for measuring the exponential divergence of originally similar state–space trajectories, are frequently used to detect chaotic behavior. The initial condition (x_0, y_0) located in the fixed

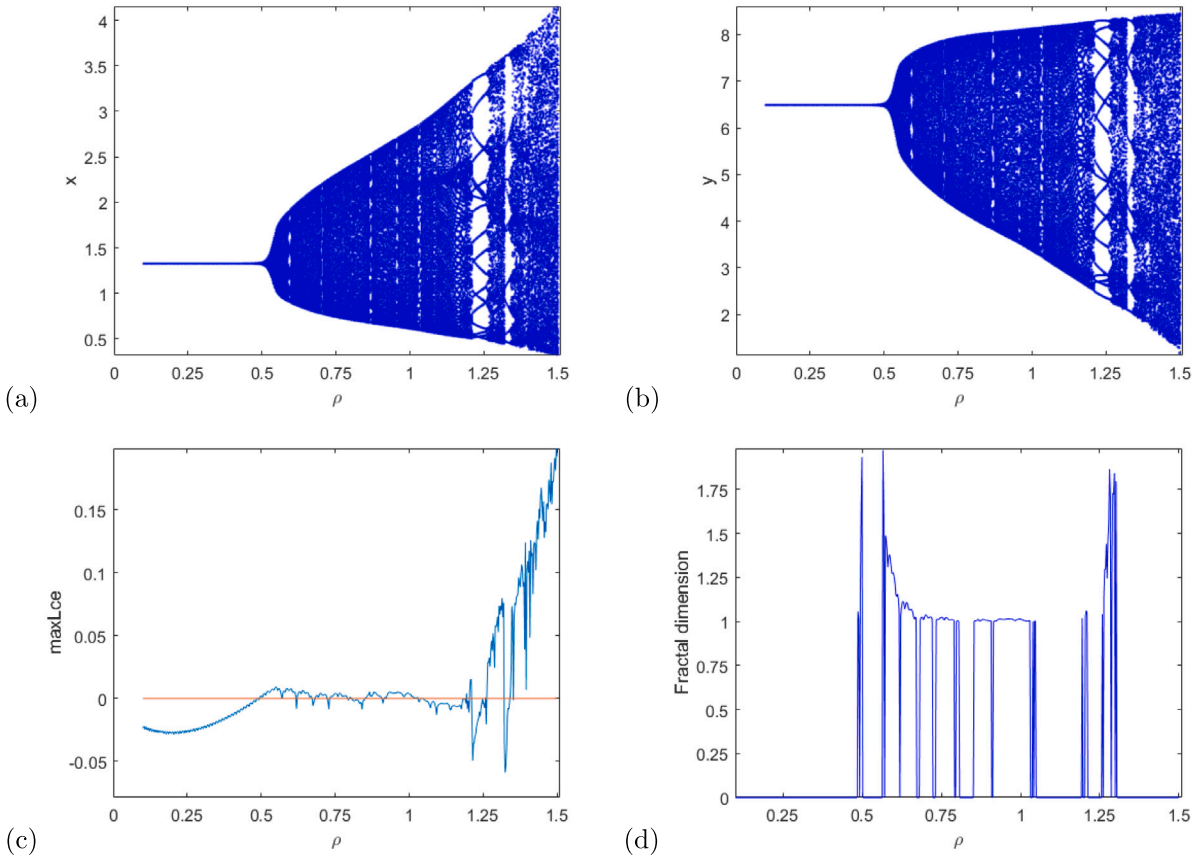

Fig. 3. Visual representation of NS Bifurcation, MLEs and FDs of species for varying parameter ρ.

point's basin of attraction can be taken into account to study the PD and NS bifurcations, respectively, for the singular positive fixed point. Based on the previous analysis, we select ρ as the bifurcation parameter. All other model parameters, unless otherwise specified, are taken as fixed parameters. For the parameters values $r = 1.5$, $k = 3.5$, $\beta = 1.05$, $a = 0.5$, $\gamma = 0.75$, $d = 0.1$, $\eta = 0.5$, $\alpha = 0.75$, and $1.4 \leq \rho \leq 2.2$, a PD bifurcation point crucial value is calculated as $\rho_F = 1.5030$ and system(5)'s co-existence fixed point has been assessed as $(3.316456152, 0.6445218958)$.

A chaotic attractor is shown to emerge from a PD bifurcation after the model track has evolved from a fixed point to a PD bifurcation displayed in Fig. 2. We also see that fixed point's (E_3) stability occurs for $\rho < \rho_F$, loses stability at $\rho > \rho_F$, and a period doubling phenomena leads to chaos at $\rho = \rho_F$. Fig. (2; c–d) shows the calculated MLEs and FDs for Fig. (2;a–b).

Next, we select the parameters values as $r = 2.25$, $k = 3.5$, $\beta = 1.05$, $a = 0.638164$, $\gamma = 0.5$, $d = 0.1$, $\alpha = 0.75$, $\eta = 0.5$, $0.1 \leq \rho \leq 1.5$ and initial condition is $(1.32, 6.5)$. For these values the co-existence fixed point of the system (5) is $(1.32771, 6.48939)$. The Neimark–Sacker bifurcation is discovered by computation as E_3 at $\rho = \rho_{NS} = 0.5$. The trajectory's development from a fixed point to an NS bifurcation and then to a chaotic attractor is shown in this Fig. 3. The phase picture, MLEs, and FDs of Fig. 3 (a-b) are shown in Figs. 4 and 3 (c–d), respectively. Each of the bifurcation mechanisms for both prey and predator has three distinct periodic windows. It proves that the dynamics of the system (5) are unexpected when the parameter ρ is changed by modest amounts. This analysis demonstrates the system's many phases, from chaos to the chaotic attractor, invariant closed curve, and stable fixed point splitting. Additionally, we researched NS bifurcation, and the corresponding NS bifurcation diagram, MLEs, and FDs are displayed in Fig. 5. This was accomplished by fixing all other parameters indicated above for Fig. 3 while altering the fractional order α in the range $0.15 \leq \alpha \leq 0.95$. The phase pictures corresponding to Fig. 5 are shown in Fig. 6.

The prey–predator model in the NS bifurcation diagram may behave more dynamically as other parameter values shift (for example, parameter γ, a). The parameter values are set to $r = 2.25$, $k = 3.5$, $\beta = 1.05$, $a = 0.638164$, $\rho = 0.5$, $d = 0.1$, $\alpha = 0.75$, $\eta = 0.5$, and γ fluctuate between $0.25 \leq \gamma \leq 0.85$ to produce a new Neimark–Sacker bifurcation diagram as shown in Fig. 9(a–b). Neimark–Sacker bifurcation occurs in the model at $\gamma = \gamma_{NS} = 0.5$. As shown in Fig. 9(a–b), another NS bifurcation diagram is created when the parameter values are set to $r = 2.25$, $k = 3.5$, $\beta = 1.05$, $\gamma = 0.5$, $\rho = 0.5$, $d = 0.1$, $\alpha = 0.75$, $\eta = 0.5$, and a varies in $0.1 \leq a \leq 0.96$. Assume that the parameters are those shown in Fig. 1. System (5) can display complicated dynamic behavior when two more parameters change through their critical levels. In the given parametric scenario, Fig. 11(a) displays the co-dimension-2 bifurcation graphs in (ρ, a, x)-space. The highest Lyapunov exponents for two control parameters is plotted in Fig. 11(b) through a 2D projection onto the (ρ, a) plane in Fig. 11(c). The dynamics of the system (5) can now be studied to understand how it transitions from a non-chaotic state to a periodic or chaotic state by determining the values of the bifurcation parameters. It is also noteworthy from Fig. 11(a) that if $\rho > 0.763701$ and parameter a increases, the predator–prey system (5) suffers PD bifurcation first and then NS bifurcation, with a stable window forming in between which is compatible with in Fig. 1(b). From a biological perspective, it illustrates how the predator and prey cohabit in an oscillating equilibrium behavior (see Figs. 7 and 8).

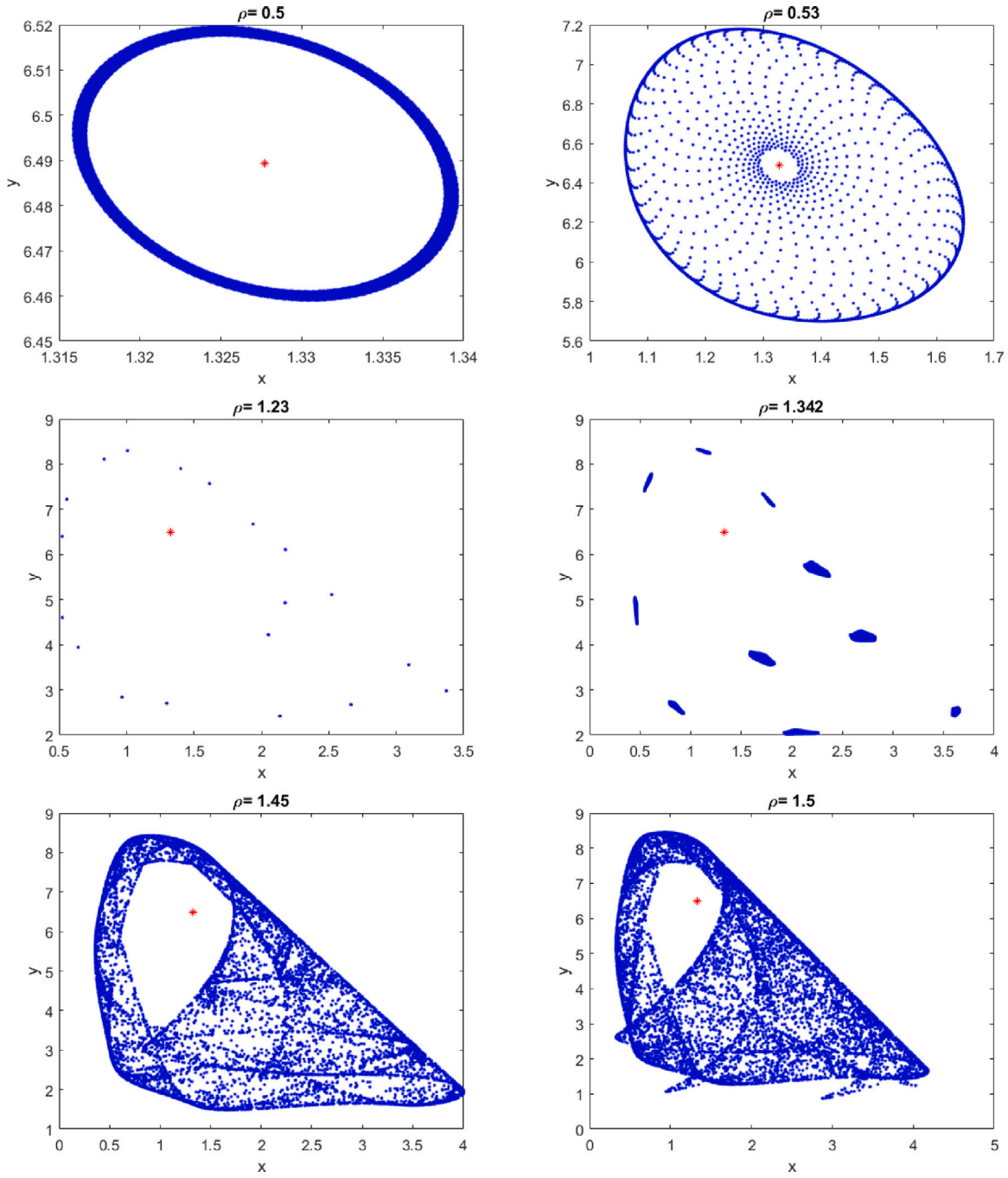

Fig. 4. Phase picture for changing input of ρ. Red $*$ represents positive fixed point. (For interpretation of the references to color in this figure legend, the reader is referred to the web version of this article.)

5.1. Fractal dimension

To identify a model's chaotic attractors, the fractal dimensions (FD) measurement is used, which is defined by [30]

$$\hat{D}_{fd} = k + \frac{\sum_{j=1}^{k} \mathrm{tt}_j}{|\mathrm{tt}_{k+1}|} \tag{17}$$

where the biggest integer number is k such that $\sum_{j=1}^{k} \mathrm{tt}_j \geq 0$ and $\sum_{j=1}^{k+1} \mathrm{tt}_j < 0$ and t_j's are Lyapunov exponents. Now, the structure of the fractal dimensions of model(5) is as follows:

$$\hat{D}_{fd} = 2 + \frac{\mathrm{tt}_1}{|\mathrm{tt}_2|} \tag{18}$$

Given that the chaotic dynamics of the model (5) (Fig. 4) are quantified with the sign of FD (Fig. 3(d)), it is guaranteed that the dynamics of the fractional order prey–predator model become unstable as the value of the parameter ρ rises.

5.2. 0–1 Chaos test algorithm

In dynamical systems, chaos refers to complex behavior characterized by sensitivity to initial conditions and aperiodic, unpredictable trajectories. Chaos tests are used to determine whether a system exhibits chaotic behavior. "0-1 chaos test" helps identify whether the predator–prey model exhibits chaotic behavior. The presence of chaos indicates that the system is complex and sensitive to initial conditions,

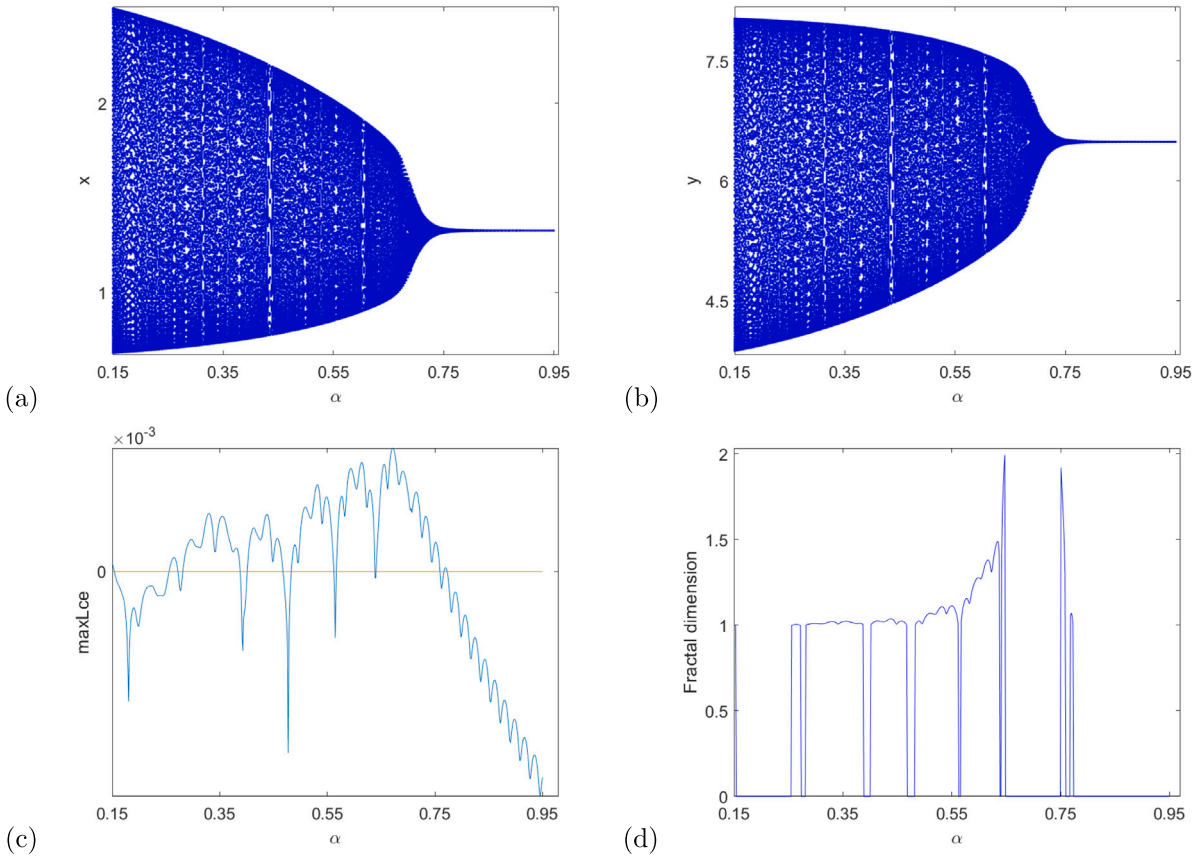

Fig. 5. Visual representation of NS Bifurcation, MLEs and FDs of species for varying parameter α.

which can have significant ecological implications. The presence of chaos in the predator–prey model can provide ecological insights. For example, it may indicate that there are multiple attractors in the system, representing different stable states of the ecosystem. However, chaos tests require data or parameter values for the predator–prey model. If accurate data is not available, or if the model parameters are estimated with uncertainties, the results of the chaos test may be less reliable. "0-1 chaos test" cannot guarantee the discovery of all possible chaotic scenarios, as it is inherently impossible to test every potential chaotic event.

Assume that $\widehat{\theta}_b(n)$ is a measured discrete set of data for the $0-1$ chaos test technique [31–33], where $n = 1, 2, 3, \ldots, N$, and the total amount of the data is N.

We generate new coordinates $(\widehat{q}_{\widehat{b}}(n), \widehat{r}_{\widehat{b}}(n))$ by choosing a random number $\widehat{b} \in (\pi/5, 4\pi/5)$ and doing the following:

$$\begin{aligned} \widehat{q}_{\widehat{b}}(n)(n) &= \sum_{j=1}^{n} \widehat{\theta}_b(j)\cos(\widehat{\phi}_b(j)) \\ \widehat{r}_{\widehat{b}}(n) &= \sum_{j=1}^{n} \widehat{\theta}_b(j)\sin(\widehat{\phi}_b(j)) \end{aligned} \tag{19}$$

where $\widehat{\phi}_b(j) = jc + \sum_{i=1}^{j} \widehat{\theta}_b(j), \quad j = 1, 2, 3, \ldots, n.$

The following definition applies to mean square displacement $C_{\widehat{b}}(n)$ as of this moment:

$$C_{\widehat{b}}(n) = \lim_{N\to\infty} \frac{1}{N} \sum_{j=1}^{N} \left(\widehat{q}_{\widehat{b}}(j+n) - \widehat{q}_{\widehat{b}}(j)\right)^2 + \left(\widehat{r}_{\widehat{b}}(j+n) - \widehat{r}_{\widehat{b}}(j)\right)^2, \quad n \in \left[1, \frac{N}{10}\right] \tag{20}$$

We also define $\check{C}_{\widehat{b}}(n)$ as the modified mean square displacement as follows:

$$\check{C}_{\widehat{b}}(n) = \check{C}_{\widehat{b}}(n) - \left(\lim_{N\to\infty} \frac{1}{N} \sum_{j=1}^{N} \widehat{\theta}_b(j)\right)^2 \frac{1-\cos n\widehat{b}}{1-\cos \widehat{b}}$$

The following description follows for the median correlation coefficient $\widehat{K}$ value:

$$\widehat{K} = \text{median}\left(\widehat{K}_{\widehat{b}}\right)$$

where

$$\widehat{K}_{\widehat{b}} = \frac{\text{cov}(\xi_1, \xi_2)}{\sqrt{\text{var}(\xi)\,\text{var}(\varphi)}} \in [-1, 1]$$

in which $\xi_1 = (1, 2, 3, \ldots, n_{cut}), \quad \xi_2 = \left(\check{C}_{\widehat{b}}(1), \check{C}_{\widehat{b}}(2), \ldots, \check{C}_{\widehat{b}}\left(n_{cut}\right)\right), n_{cut} = \text{round}\left(\frac{N}{10}\right)$, and covariance and variance of vectors of length $\bar{n}$ are defined as follows:

$$\text{cov}(x, y) = \frac{1}{\bar{n}} \sum_{j=1}^{\bar{n}} (x(j) - \bar{x})(y(j) - \bar{y}),$$

$$\bar{x} = \frac{1}{\bar{n}} \sum_{j=1}^{\bar{n}} x(j),$$

$$\text{var}(x) = \text{cov}(x, x).$$

The output can now be demonstrated as follows.

(i) The dynamics remain stable (i.e., periodic or quasi-periodic) when $\widehat{K} \approx 0$, whereas $\widehat{K} \approx 1$ suggests that the dynamics are chaotic.

(ii) As opposed to Brownian-like (unbounded) trajectories, which show chaotic dynamics, bounded trajectories on the $(\widehat{q}, \widehat{r})$ plane show regular dynamics (i.e., periodic or quasi-periodic dynamics).

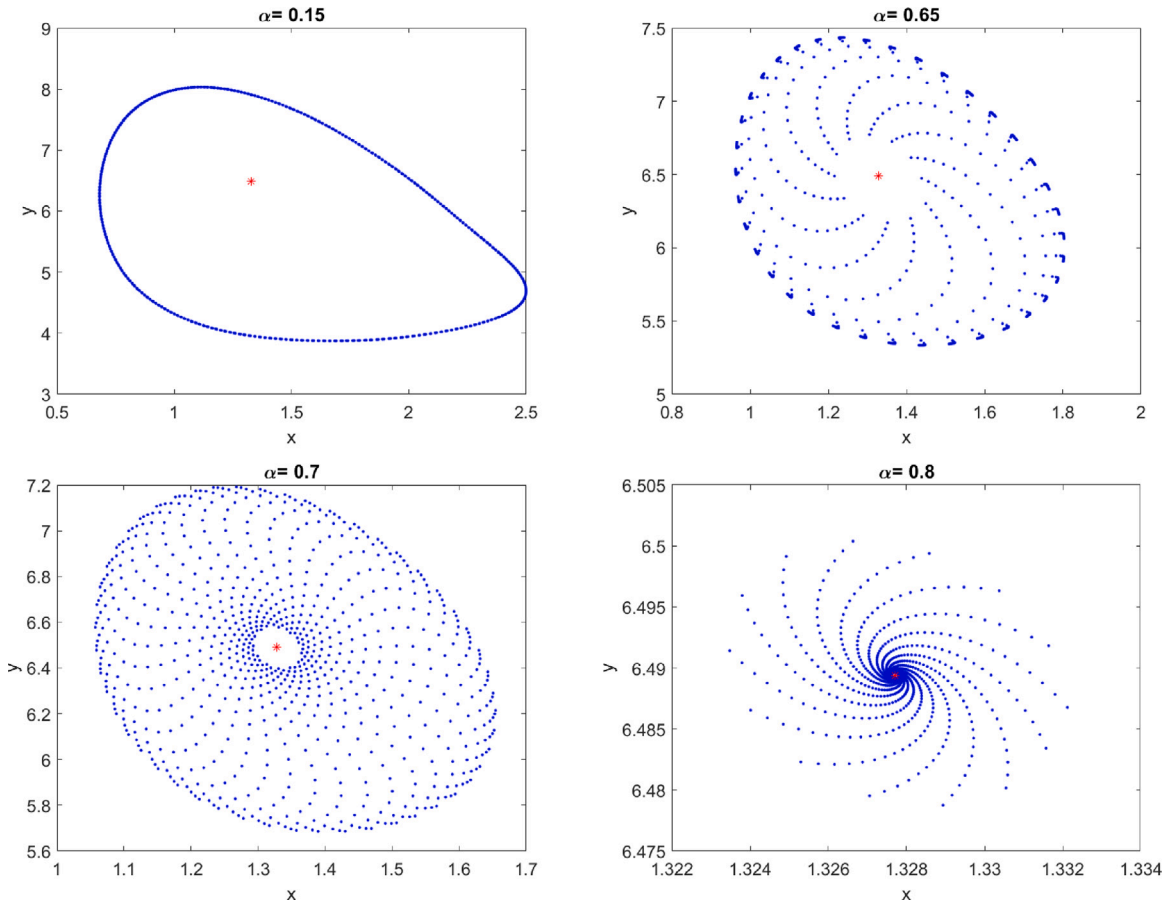

Fig. 6. Phase picture for changing input of α. Red $*$ represents positive fixed point. (For interpretation of the references to color in this figure legend, the reader is referred to the web version of this article.)

Example. Select the parameter values so that $r = 2.25$, $k = 3.5$, $\beta = 1.05$, $a = 0.638164$, $\gamma = 0.5$, $d = 0.1$, $\alpha = 0.75$, $\eta = 0.5$, $\rho = 1.5$ with $K = 0.91144$, the Brownian-like (unbounded) trajectories in new coordinates$(\hat{q}, \hat{w})$−plane displaying in Fig. 10(a) are compatible with a chaotic system dynamics. The curve $\widehat{K}$ versus ρ plotted in Fig. 10(b) represents the correlation coefficient value. In terms of biology, it means that the system is chaotic for parameter k values where K is near to 1.

6. Chaos control

The four methodologies for studying chaos control in discrete-time models that are most frequently cited when addressing the issue of managing chaos are the state feedback method, pole-placement methodology, OGY technique, and hybrid control approach. To control chaos emerging from the Neimark–Sacker bifurcation, the OGY feedback control method strategy [34] and state feedback [35] are applied to the system (5), and the parameter ρ as a control parameter is used. We write system (5) as:

$$\begin{aligned} x_{n+1} &= x_n + \frac{\Lambda^\alpha}{\Gamma(\alpha+1)}\left(r x_n\left(1-\frac{x_n}{k}\right) - \eta\left(1-e^{-a x_n}\right) y_n\right) = f(x_n, y_n, \rho_c) \\ y_{n+1} &= y_n + \frac{\Lambda^\alpha}{\Gamma(\alpha+1)}\left(\beta\left(1-e^{-a x_n}\right) y_n - d y_n - \gamma y_n\right) = g(x_n, y_n, \rho_c), \end{aligned} \tag{21}$$

where the control force $\Lambda := \rho - p_1\left(x_n - x^*\right) - p_2\left(y_n - y^*\right)$, is specified as the feedback gains p_1 and p_2, and (x^*, y^*) is the interior fixed point for the system(5). The specific number of ρ_c indicates that the interval is chaotic or bifurcating, that is, $\rho_c \geq \rho_-$ or $\rho_c \geq \rho_{NS}$. Additionally, ρ is constrained to exist in a small interval $|\rho - \rho_0| < \mu$ with $\mu > 0$ and ρ_0 designating the nominal value belonging to chaotic area. To change the trajectory and bring it closer to the intended orbit, we employ the stabilizing feedback control strategy. In the chaotic region created by the emergence of Neimark–Sacker bifurcation, we suppose that (x^*, y^*) is an unstable fixed point of the system (5). The system (21) can then be approximated in the vicinity of the unstable fixed point (x^*, y^*) by the following linear map:

$$\begin{bmatrix} x_{n+1} - x^* \\ y_{n+1} - y^* \end{bmatrix} \approx A \begin{bmatrix} x_n - x^* \\ y_n - y^* \end{bmatrix} + B\left[\rho - \rho_0\right], \tag{22}$$

where

$$\begin{aligned} A_{(x^*,y^*,\rho_0)} &= \begin{bmatrix} \frac{\partial f(x^*,y^*,\rho_0)}{\partial x} & \frac{\partial f(x^*,y^*,\rho_0)}{\partial y} \\ \frac{\partial g(x^*,y^*,\rho_0)}{\partial x} & \frac{\partial g(x^*,y^*,\rho_0)}{\partial y} \end{bmatrix} \\ &= \begin{bmatrix} \widetilde{\beta_a \beta_a} & -\frac{\eta\rho_0(d+\gamma)}{\beta\Gamma(\alpha+1)} \\ \frac{\beta r\rho_0(-\beta+d+\gamma)}{ak\eta(d+\gamma)\Gamma(\alpha+1)} \ln\left(\frac{\beta-d-\gamma}{\beta}\right)(ak + \ln\left(\frac{\beta-d-\gamma}{\beta}\right)) & 1 \end{bmatrix}, \end{aligned}$$

where $\widetilde{\beta_a \beta_a} = 1 + \frac{r\rho_0}{\Gamma(\alpha+1)} + 2\frac{r\rho_0}{ak\Gamma(\alpha+1)} \ln\left(\frac{\beta-d-\gamma}{\beta}\right) + \frac{r\rho_0(-\beta+d+\gamma)}{ak(d+\gamma)\Gamma(\alpha+1)} \ln\left(\frac{\beta-d-\gamma}{\beta}\right)(ak + \ln\left(\frac{\beta-d-\gamma}{\beta}\right))$ and

$$\begin{aligned} B_{(x^*,y^*,\rho_c)} &= \begin{bmatrix} \frac{\partial f(x^*,y^*,\rho_c)}{\partial \rho} \\ \frac{\partial g(x^*,y^*,\rho_c)}{\partial \rho} \end{bmatrix} \\ &= D \begin{bmatrix} -a\left(ak - 2 + (ak + \ln\left(\frac{\beta-d-\gamma}{\beta}\right)(d+z))\right) \\ 0 \end{bmatrix}, \end{aligned}$$

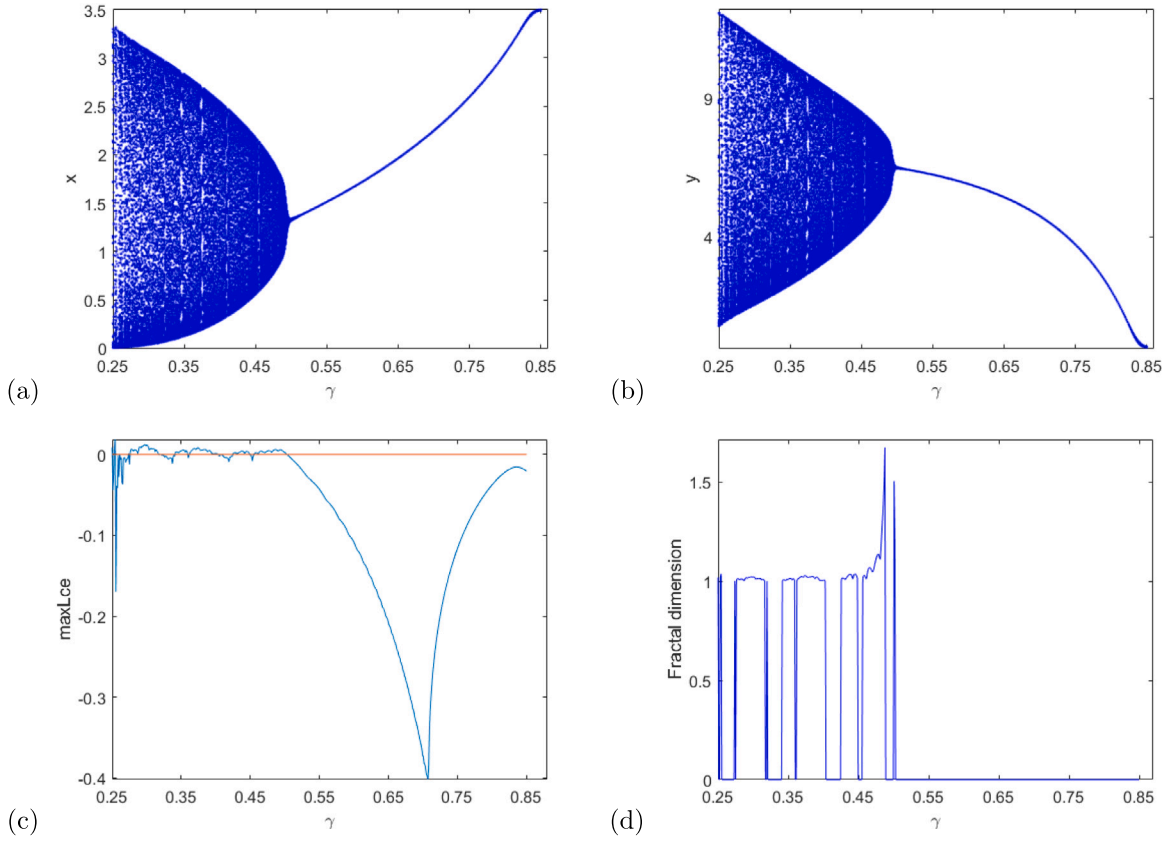

Fig. 7. Visual representation of NS Bifurcation, MLEs and FDs of species for varying parameter γ.

$$D := \frac{\rho_c r \ln(\frac{\beta-d-\gamma}{\beta})}{\Gamma(\alpha+1)\rho_c a^2 k}.$$

By arguing as in [?], it can be say that the system (21) is controllable the following matrix C:

$$C = \left[B_{(x^*,y^*,\rho_c)} : A_{(x^*,y^*,\rho_c)} B_{(x^*,y^*,\rho_c)}\right]$$

Because, the controllable matrix C is of rank 2. The fixed point (x^*, y^*) of Eq. (22) is then locally asymptotically stable if and only if both of the eigenvalues of the matrix $A - BK$ are located in an open unit disk. We suppose that $\left[\rho - \rho_0\right] = -K \begin{bmatrix} x_n - x^* \\ y_n - y^* \end{bmatrix}$, where $K = [p_1\ p_2]$, then the system (22) can be written as follow:

$$\begin{bmatrix} x_{n+1} - x^* \\ y_{n+1} - y^* \end{bmatrix} \approx [A - BK] \begin{bmatrix} x_n - x^* \\ y_n - y^* \end{bmatrix}. \tag{23}$$

The following is the jacobian matrix's $A - BK$ characteristic equation:

$$P(\lambda) = \lambda^2 - (tr(A - BK))\,\lambda + \det(A - BK) = 0. \tag{24}$$

Considering that λ_1 and λ_2 are the solutions of the characteristic Eq. (24),

$$\begin{aligned}\lambda_1 + \lambda_2 &= \frac{\widetilde{\mu_e}\alpha r}{\rho a} \ln\left(\frac{\beta-d-\gamma}{\beta}\right)\left[1 + \frac{\ln\left(\frac{\beta-d-\gamma}{\beta}\right)}{ak} + \frac{\beta\left(ka+\ln\left(\frac{\beta-d-\gamma}{\beta}\right)\right)}{ak(d+z)}\right.\\ &\left. + \left(ka + \ln\left(\frac{\beta-d-\gamma}{\beta}\right)\right)\frac{(-\beta+d+\gamma)}{ak(d+z)}\right] p_1 + 2 + \widetilde{\mu_e} r\\ &+ \frac{\widetilde{\mu_e} r}{ka} \ln\left(\frac{\beta-d-\gamma}{\beta}\right)\left(2 + \frac{ka+\ln\left(\frac{\beta-d-\gamma}{\beta}\right)}{(d+z)}\right)(-\beta+d+\gamma),\end{aligned}$$

$$\begin{aligned}\lambda_1\lambda_2 &= 2\widetilde{\mu_e}\alpha r \ln\left(\frac{\beta-d-\gamma}{\beta}\right)\left(\frac{ka+1}{ka^2\rho}\right) p_1\\ &+ \frac{2(\widetilde{\mu_e} r)^2 \alpha\beta}{\eta(d+\gamma)k^2a^3\rho} \ln\left(\frac{\beta-d-\gamma}{\beta}\right)(d+\gamma-\beta)(a^2k^2\\ &+ \ln\left(\frac{\beta-d-\gamma}{\beta}\right)\left(2ka + \ln\left(\frac{\beta-d-\gamma}{\beta}\right)\right))p_2\\ &+ 1 + \widetilde{\mu_e} r + \frac{\widetilde{\mu_e} r}{ka(d+\gamma)} \ln\left(\frac{\beta-d-\gamma}{\beta}\right)(ka(d+\gamma-\beta) + 2(d+\gamma) + \gamma)\\ &+ \frac{(\widetilde{\mu_e})^2 r}{ka(d+\gamma)} \ln\left(\frac{\beta-d-\gamma}{\beta}\right)\left((ak+1)\left(\gamma\beta - \gamma^2 - d^2\right) + dak(\beta-2\gamma)\right)\\ &+ \frac{\widetilde{\mu_e} r}{ka(d+\gamma)}\left(\ln\left(\frac{\beta-d-\gamma}{\beta}\right)\right)^2\left((-a\beta+d) + \widetilde{\mu_e} da(\beta-\gamma)\right)\end{aligned} \tag{25}$$

are obtained. Equations $\lambda_1 = \pm 1$ and $\lambda_1\lambda_2 = 1$ must be solved to determine the lines of marginal stability. These limitations ensure that λ_1 and λ_2 have precise values that are less than 1. If $\lambda_1\lambda_2 = 1$, then the second portion of Eq. (25) implies that

$$\begin{aligned}L_1 := &\frac{2\widetilde{\mu_e}\alpha r}{ka^2\rho}(ka+2)\ln\left(\frac{\beta-d-\gamma}{\beta}\right) p_1\\ &+ \frac{4(\widetilde{\mu_e})^2\alpha\beta r^2}{\eta k^2 a^3 \rho(d+\gamma)}(-\beta+d+\gamma)(ka+2)(ka+1)\ln\left(\frac{\beta-d-\gamma}{\beta}\right) p_2\\ &+ \widetilde{\mu_e} r - 2(\beta - 2d - 2\gamma)\\ &+ \widetilde{\mu_e} r(\beta - d - \gamma)\ln\left(\frac{\beta-d-\gamma}{\beta}\right)\left(\widetilde{\mu_e}(ka+2)(\gamma+d) + ka\right) = 0\end{aligned}$$

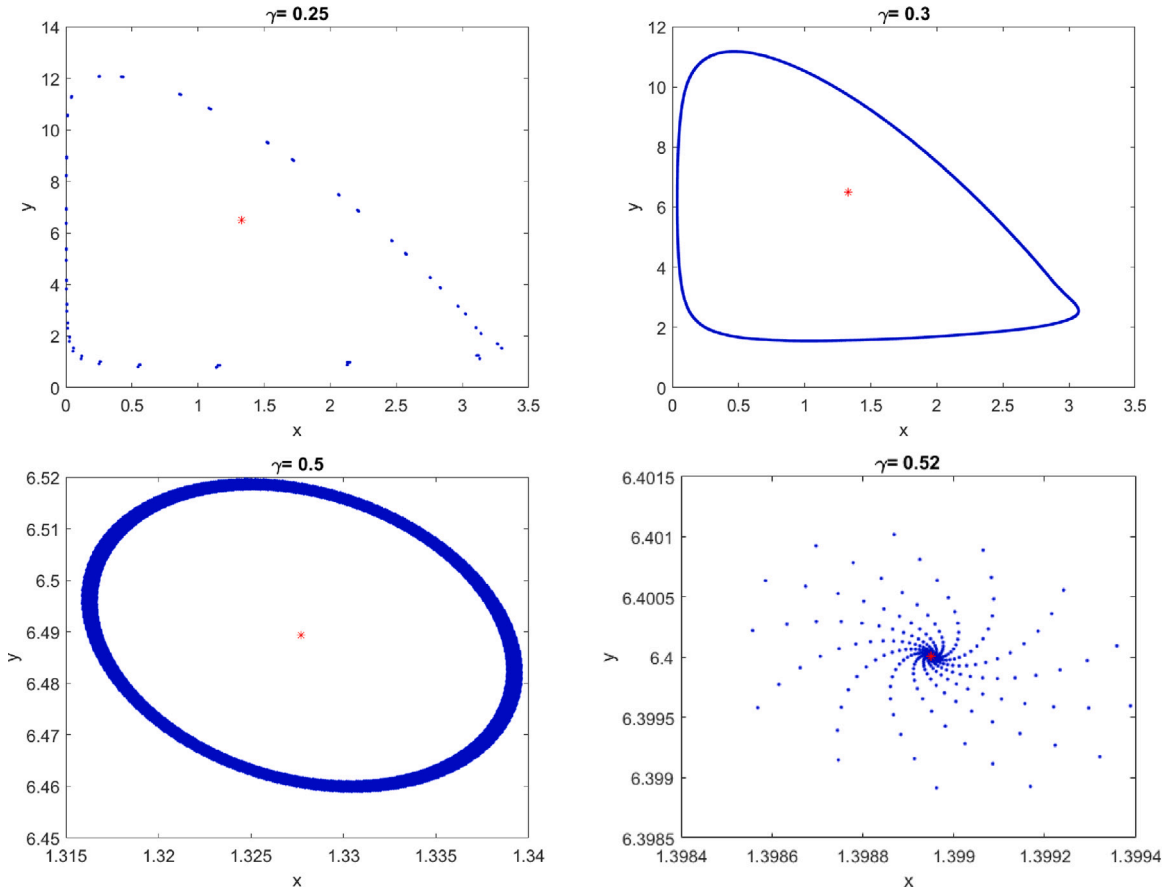

Fig. 8. Phase picture for changing input of γ. Red $*$ represents positive fixed point. (For interpretation of the references to color in this figure legend, the reader is referred to the web version of this article.)

Moreover, we suppose that $\lambda_1 = 1$, then using the equations (25) yield that

$$
\begin{aligned}
L_2 := \quad & \frac{2\widetilde{\mu_e}\alpha r}{ka^2}\ln\left(\frac{\beta-d-\gamma}{\beta}\right)\left(2(ka+2)-\frac{2(ka+1)+\ln\left(\frac{\beta-d-\gamma}{\beta}\right)}{\rho}\right)p_1 \\
& + \frac{4\widetilde{\mu_e}\alpha\beta r^2}{\eta(d+\gamma)k^2a^3}\ln\left(\frac{\beta-d-\gamma}{\beta}\right)(-\beta+\gamma+d)(ka+2)(ka+1)\,p_2 \\
& + \frac{\widetilde{\mu_e}r}{ka(d+\gamma)}\ln\left(\frac{\beta-d-\gamma}{\beta}\right)(2(-\beta+2\gamma+2d)+ka(-\beta+\gamma+d) \\
& + \widetilde{\mu_e}ka\gamma((\beta-d-\gamma)+2\gamma(\beta-\gamma)-d^2(2\eta+ka) \\
& + d(-4\gamma+ka+2\beta))) \\
& - \frac{\widetilde{\mu_e}r}{ka(d+\gamma)}\ln\left(\frac{\beta-d-\gamma}{\beta}\right)(2(d+\gamma) \\
& + (-\beta+\gamma+d)\left(ka+\ln\left(\frac{\beta-d-\gamma}{\beta}\right)\right)\Big)
\end{aligned}
$$

Finally, taking $\lambda_1 = -1$ and using Eqs. (25) we get

$$
\begin{aligned}
L_3 := \quad & 4+2\widetilde{\mu_e}r \\
& + \left(ka+\ln\left(\frac{\beta-d-\gamma}{\beta}\right)\right)\ln\left(\frac{\beta-d-\gamma}{\beta}\right)((1-\beta+d+\gamma)\,p_1 \\
& + (-\beta+d+\gamma)\,a) \\
& + \ln\left(\frac{\beta-d-\gamma}{\beta}\right)\left[\frac{3\alpha}{a\rho}p_1+\frac{2}{ak}+\frac{\widetilde{\mu_e}r}{(d+\gamma)k}(2\gamma+ak(\gamma-\beta)+3kd)\right. \\
& + \widetilde{\mu_e}(d+\gamma)(-\beta+d+\gamma) \\
& + 4\frac{(\widetilde{\mu_e})^2\alpha\beta r^2}{\eta k^2a^3\rho(d+\gamma)}(-\beta+d+\gamma)(3ka+2)\,p_2 \\
& + 2\frac{\widetilde{\mu_e}r}{\eta(d+\gamma)ka^2\rho}\left((-\beta+d+\gamma)\eta a+3\eta(d+\gamma)\,p_1\right. \\
& + \widetilde{\mu_e}r\left(2ka\alpha\beta(-\beta+d+\gamma)\,p_2\right. \\
& + \left.\left.\frac{a\eta}{r}(-\gamma(\gamma+2d)+\beta(d+1))\right)\right]
\end{aligned}
$$

In that case, stable eigenvalues are found in the triangle in the p_1p_2 plane circumscribed by the lines L_1, L_2, L_3 for a given parametric values.

State feedback control, a method, is used to stabilize chaos at the moment where the system's (5) unstable paths begin. The system (5) can be made to take on a controlled form by introducing a feedback control law as the control force u_{bb} and using the following formula.

$$
\begin{aligned}
x_{n+1} &= x_n + \frac{\rho^\alpha}{\Gamma(\alpha+1)}\left(rx_n\left(1-\frac{x_n}{k}\right)-\eta(1-\exp(-ax_n))y_n\right)+u_{bb} \\
y_{n+1} &= y_n + \frac{\rho^\alpha}{\Gamma(\alpha+1)}\left(\eta(1-\exp(-ax_n))y_n - dy_n - \gamma y_n\right) \\
u_{bb} &= -k_1(x_n-x^*)-k_2(y_n-y^*)
\end{aligned}
\tag{26}
$$

where (x^*, y^*) represents the non-negative fixed point of the system (5). The values k_1 and k_2 indicate the feedback gains.

Example. We take $(\rho, r, k, \beta, a, \gamma, d, \alpha, \eta) = (2.000199345, 1.5, 9.2, 0.77, 0.5, 0.5, 0.2, 0.9, 0.8)$. Thus the co-existence fixed point of the system (5) is $(4.795790546, 4.735156114)$. The specified controlled system is provided

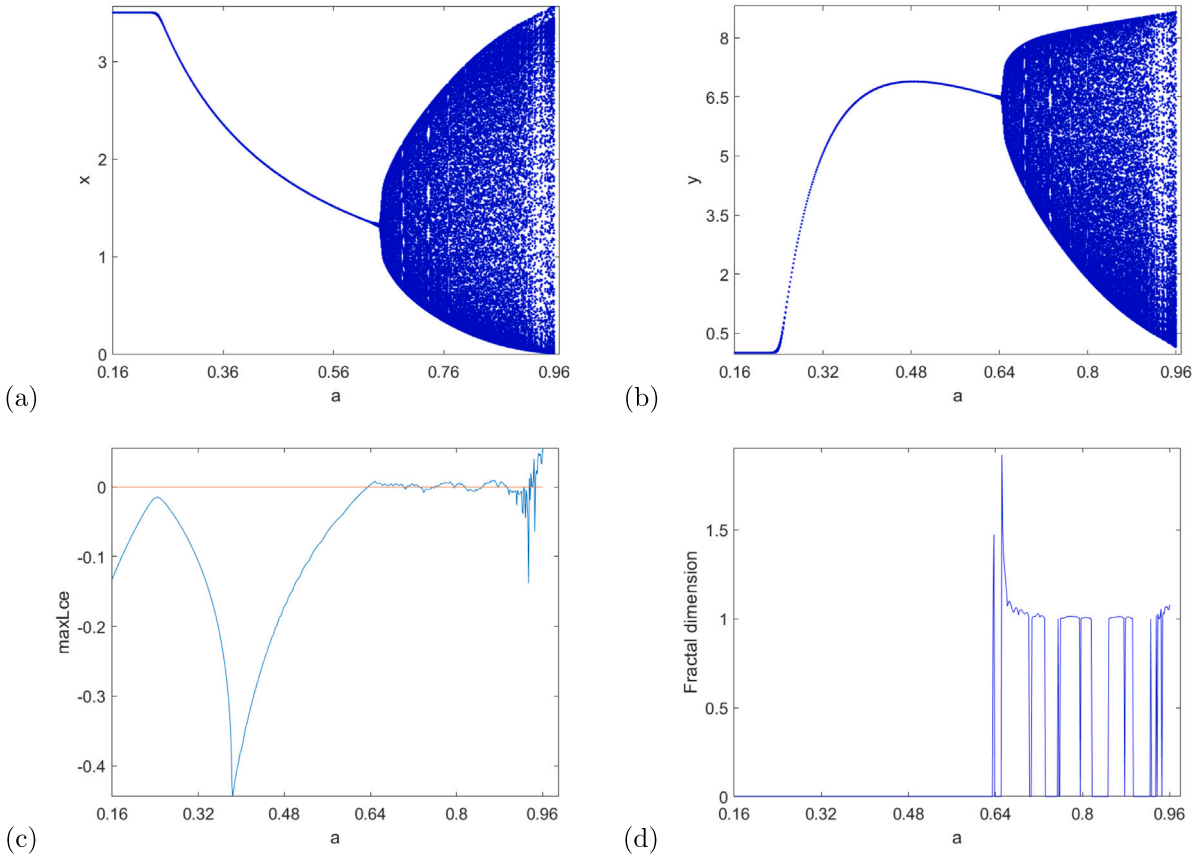

Fig. 9. Visual representation of NS Bifurcation, MLEs and FDs of species for varying parameter a.

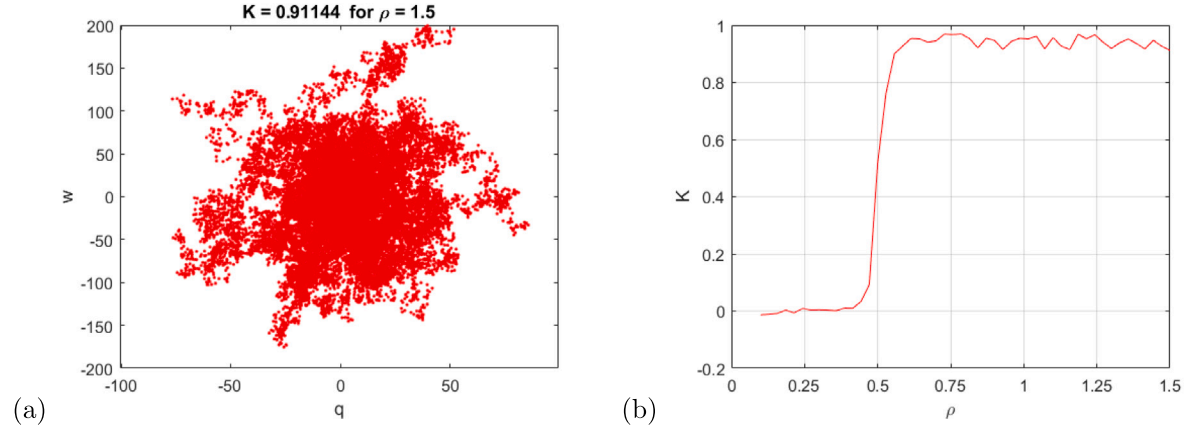

Fig. 10. $0-1$ chaos test for model (5). (a) q versus w (b)Plot in new coordinates (ρ, K) plane .

by:

$$\begin{aligned} x_{n+1} = \; & x_n + \omega(1.5(x_n - 4.795790546)(1 - (x_n - 4.795790546)/9.2)) \\ & - \omega(0.8(1 - exp(-0.4(x_n - 4.795790546)))(y_n - 4.735156114)) \\ y_{n+1} = \; & y_n + \omega(0.77(1 - exp(-0.4(x_n - 4.795790546))(y_n - 4.735156114) \\ & - 0.7(y_n - 4.735156114))). \end{aligned} \tag{27}$$

where $\omega := (2.000199345)^{0.9}/0.9617658319$, $K = \begin{bmatrix} p_1 & p_2 \end{bmatrix}$ be gain matrix and $(x^*, y^*) = (4.795790546, 4.735156114)$ is the fixed point of the system (5) which leads the system to an unstable situation. Also, we have

$$A = \begin{bmatrix} 1.247696937 & -1.662715998 \\ -0.3788987037 & 1 \end{bmatrix},$$

$$B = \begin{bmatrix} 5.904914872 \\ 0 \end{bmatrix},$$

and

$$C = [B : AB] = \begin{bmatrix} 5.904914872 & 7.367544199 \\ 0 & -2.237364590 \end{bmatrix}.$$

It is then simple to verify that the C matrix's rank is 2. As a result, the system (27) is manageable. Next, the regulated system's (27) jacobian matrix $A - BK$ is provided by

$$A - BK$$

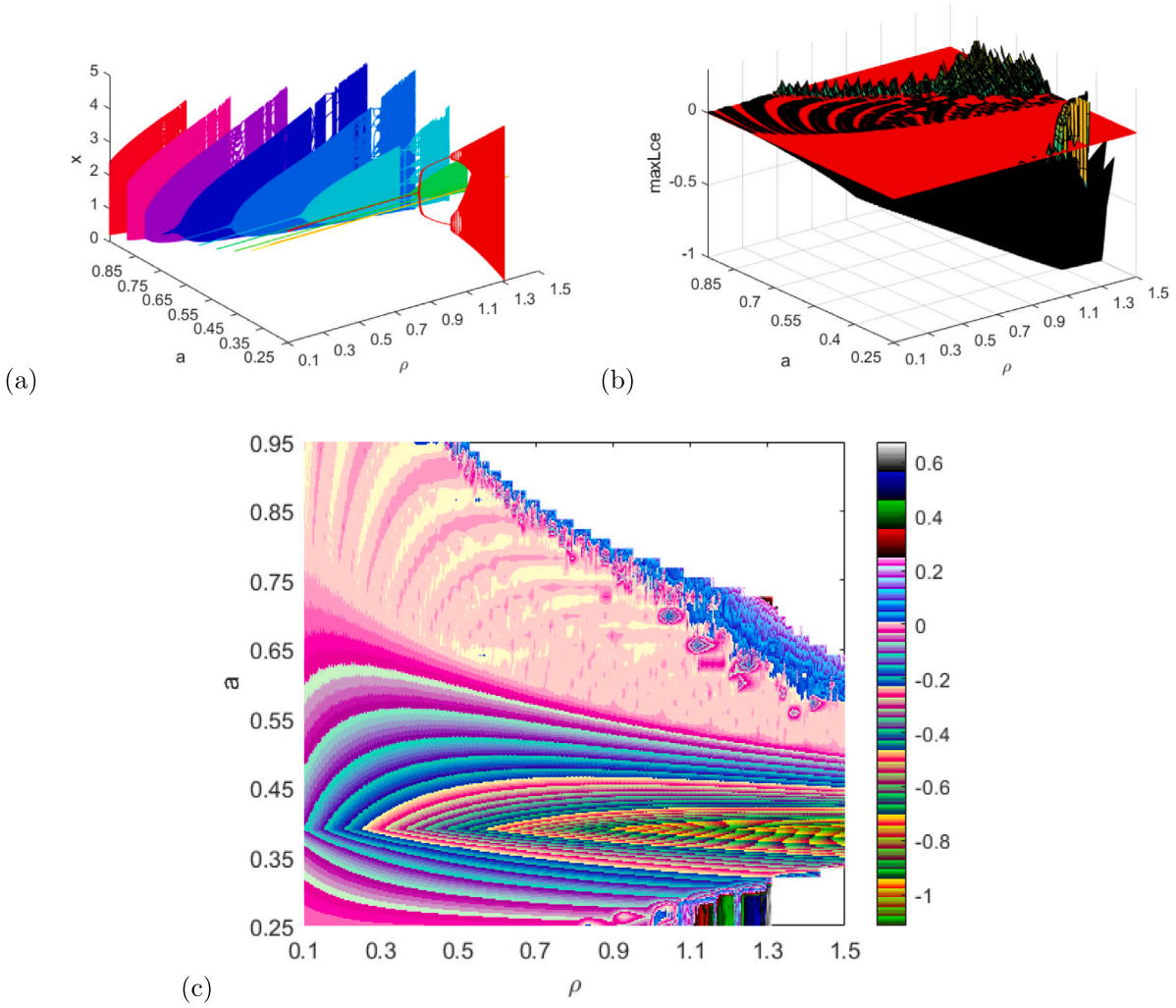

Fig. 11. (a) 3D Bifurcation diagram in (ρ, a, x) space (b) 3D MLE (c) Maximum Lyapunov exponents projected in (ρ, a) plane.

$$= \begin{bmatrix} 1.247696937 - 5.904914872p_1 & -1.662715998 - 5.904914872p_2 \\ -0.3788987037 & 1 \end{bmatrix} \tag{28}$$

Moreover, the lines L_1, L_2 and L_3 which represent the marginal stability and given by:

$$L_1 = -0.3823039998 - 5.904914872p_1 - 2.237364592p_2,$$

$$L_2 = -0.630000937 - 2.237364592p_2 = 0,$$

and

$$L_3 = 3.865392937 - 11.80982974p_1 - 2.237364592p_2 = 0.$$

The stable triangular area for the controlled system (27) is then depicted in Fig. 12(i) and is bounded by the marginal lines L_1, L_2 and L_3.

We conducted numerical simulations(see Fig. 12)(ii) to study how the state feedback control influence functions as a chaos controller in an unstable environment. The parameters will be set to the same values as the OGY method that we choose except $\rho = 1.5$. The selected feedback gains are $k_1 = 0.75$ and $k_2 = -0.01$.

7. Conclusions

In this study, the dynamics of a discrete prey–predator model with harvesting in fractional order are examined. Three fixed points are discovered under specific parametric circumstances and the article goes into great detail about the stability of these fixed points. We demonstrate mathematically and numerically that the model system can undergo period-doubling and Neimark–Sacker bifurcations in certain conditions. We notice that the stability of the fixed points is greatly influenced by the model parameters. Notably, our findings indicate that chaotic behavior is visible in the model and the system destabilizes as the parameters ρ, a, rise, causing a split from a stable state to chaotic behavior. We also observe how the model's behavior is impacted by harvesting. For instance, more significant predator harvesting results in unstable model dynamics, whereas lower predator harvesting stabilizes the model dynamics. The numerical simulation demonstrates that two parameters have changed simultaneously to exhibit the model's intricate dynamics. We construct multiple bifurcation diagrams and the largest Lyapunov exponent in both 3D and 2D diagrams by varying ρ and a. Interesting dynamical characteristics are seen in two-parameter spaces that cannot be discovered by focusing on a single parameter alone. The presence of different bifurcations exposes the dynamic behavior of the discrete model with differing complexity from diverse perspectives. For instance, the Neimark–Sacker bifurcation starts a path to chaos by causing a dynamic change from a stable fixed point to attractive cycles and causes complicated dynamics, such as periodic windows and chaotic attractors, to emerge. Populations with erratic oscillations may abruptly change to ones with regular oscillations due to environmental changes. The invariant curve in the supercritical

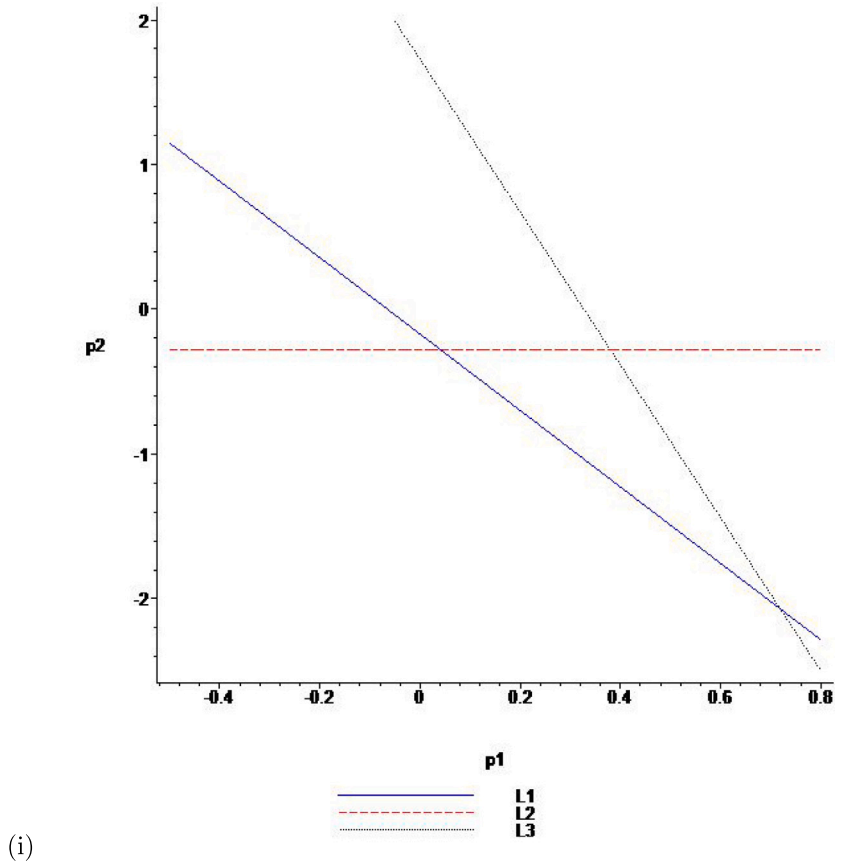

(i)

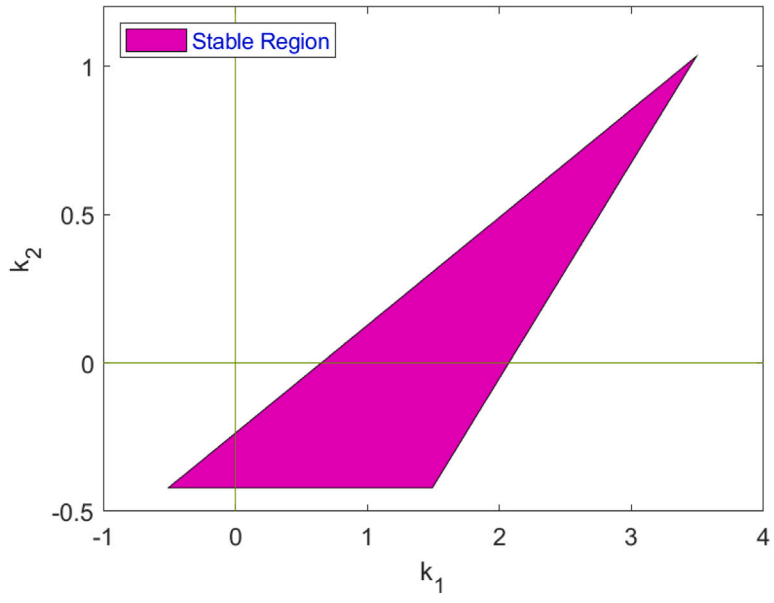

(ii)

Fig. 12. Stable regions: (i) OGY method, (ii) State feedback method.

Neimark–Sacker bifurcation provides important insights into the dynamics of nonlinear systems near the critical point. It reveals how the system's behavior changes as the parameter varies, and it plays a key role in understanding the transition from stable periodic motion to more complex and chaotic dynamics. In ecology, an invariant closed curve for supercritical NS, denotes the possibility of coexistence and self-production of densities for both predator and prey. On the invariant curve, there could be periodic or quasi-periodic dynamics. The model exhibits a period-doubling bifurcation, demonstrating the evolution of the prey and predator populations. The period-doubling bifurcation is associated with the emergence of chaotic behavior from a stable periodic solution. It demonstrates the richness and ubiquity of chaotic behavior in various natural phenomena and systems. We also present the applicability of the OGY and state feedback techniques to control chaotic behavior, both numerically and analytically.

Our main finding is that the system's behavior is significantly impacted by the amount of memory that the parameter α represents. Our research indicates that weak memory, which is denoted by a α value that is approaching 1, resulting in erratic behavior, yet having a strong memory, which is represented by an α value that is getting closer to zero, stabilizes the system. These findings emphasize how important memory is to the behavior of the model.

Finally, this study offers a comprehensive analysis of the dynamics of the model and shows how bifurcations and chaos can occur when certain parametric conditions are met. We also highlight how memory affects system behavior. Our research advances knowledge of the model's dynamics and highlights the function that memory plays in the behavior of the model.

Funding

This study effort has no funding.

CRediT authorship contribution statement

Md. Jasim Uddin: Methodology, Computations, Analysis, Validation, Writing – original draft, Review & editing. **Sarker Md. Sohel Rana:** Conceptualization, Software, Resources, Supervision, Writing – original draft, Review & editing. **Seval Işık:** Methodology, Investigation, Writing – original draft, Review & editing. **Figen Kangalgil:** Conceptualization, Supervision, Writing – original draft, Review & editing.

Declaration of competing interest

There are no competing interests, according to the writers.

Data availability

No data was used for the research described in the article

References

[1] Suryanto A, Darti I, Panigoro HS, Kilicman A. A fractional-order predator–prey model with ratio-dependent functional response and linear harvesting. Mathematics 2019;7(11):1100.
[2] Lotka AJ. Elements of physical biology. Baltimor: Williams & Wilkins; 1925.
[3] Volterra V. Variazioni e fluttuazionidelnumero di indivui in species animaliconviventi. Mem Accad Naz Lincei 1926;2:31–313.
[4] Liu B, Zhang Y, Chen L. Dynamic complexities in a Lotka–Volterra predator–prey model concerning impulsive control strategy. Int J Bifurcation Chaos 2005;15(2):517–31.
[5] Xiao D, Ruan S. Global analysis in a predator–prey system with nonmonotonic functional response. SIAM J Appl Math 2001;61(4):1445–72.
[6] Agiza HN, Elabbasy EM, El-Metwally H, Elsadany AA. Chaotic dynamics of a discrete prey-predator model with Holling type II. Nonlinear Anal RWA 2009;10(1):116–29.
[7] Din Q. Complexity and chaos control in a discrete-time prey-predator model. Commun Nonlinear Sci Numer Simul 2017;49:113–34.
[8] Layek GC, et al. An introduction to dynamical systems and chaos, 449. Springer; 2015.
[9] Holling CS. The functional response of predators to prey density and its role in mimicry and population regulation. Mem Entomol Soc Can 1965;97(S45):5–60.
[10] Iviev VS. Experimental ecology of the feeding of fishes. Yale Univ; 1961.
[11] Preedy KF, Schofield PG, Chaplain MA, Hubbard SF. Disease induced dynamics in host-parasitoid systems: chaos and co-existence. J R Soc Interface 2007;4(14):463–71.
[12] Guo G, Li B, Lin X. Qualitative analysis on a predator–prey model with Ivlev functional response. Adv Difference Equ 2013;2013(1):1–14.
[13] Uriu K, Iwasa Y. Turing pattern formation with two kinds of cells and a diffusive chemical. Bull Math Biol 2007;69(8):2515–36.
[14] Seval I, Kangalgil F. On the analysis of stability, bifurcation, and chaos control of discrete-time predator–prey model with Allee effect on predator. Hacet J Math Stat 2022;1–21.
[15] Khan MS, Samreen M, Gómez-Aguilar JF, Pérez-Careta E. On the qualitative study of a discrete-time phytoplankton-zooplankton model under the effects of external toxicity in phytoplankton population. Heliyon 2022;8(12):e12415.
[16] Baek H. Complex dynamics of a discrete-time predator–prey system with Ivlev functional response. Math Probl Eng 2018;2018.
[17] Layek GC, Pati NC. Organized structures of two bidirectionally coupled logistic maps. Chaos 2019;29(9):093104.
[18] Pati NC, Layek GC, Pal N. Bifurcations and organized structures in a predator–prey model with hunting cooperation. Chaos Solitons Fractals 2020;140:110184.
[19] Lee J, Baek H. Dynamics of a Beddington–DeAngelis type predator–prey system with constant rate harvesting. Electron J Qual Theory Differ Equ 2017;2017(1):1–20.
[20] Chatibi Y, El Kinani EH, Ouhadan A. Variational calculus involving nonlocal fractional derivative with Mittag–Leffler kernel. Chaos Solitons Fractals 2019;118:117–21.
[21] Fan Y, Huang X, Wang Z, Li Y. Nonlinear dynamics and chaos in a simplified memristor-based fractional-order neural network with discontinuous memductance function. Nonlinear Dynam 2018;93(2):611–27.
[22] Mondal S, Lahiri A, Bairagi N. Analysis of a fractional order eco-epidemiological model with prey infection and type 2 functional response. Math Methods Appl Sci 2017;40(18):6776–89.
[23] Uddin MJ, Rana SM. Chaotic dynamics of the fractional order Schnakenberg model and its control. Math Appl Sci Eng 2023;4(1):40–60.
[24] El-Saka HAA. Backward bifurcations in fractional-order vaccination models. J Egyptian Math Soc 2015;23(1):49–55.
[25] Yan Y, Kou C. Stability analysis for a fractional differential model of HIV infection of CD4+ T-cells with time delay. Math Comput Simulation 2012;82(9):1572–85.
[26] Javidi M, Nyamoradi N. Dynamic analysis of a fractional order prey-predator interaction with harvesting. Appl Math Model 2013;37(20–21):8946–56.
[27] Atangana A, Secer A, et al. A note on fractional order derivatives and table of fractional derivatives of some special functions. Abstr Appl Anal 2013;2013.
[28] Salman SM, Yousef AM, Elsadany AA. Stability, bifurcation analysis and chaos control of a discrete predator–prey system with square root functional response. Chaos Solitons Fractals 2016;93:20–31.
[29] Khan MS. Bifurcation analysis of a discrete-time four-dimensional cubic autocatalator chemical reaction model with coupling through uncatalysed reactant. MATCH Commun Math Comput Chem 2022;87(2):415–39.
[30] Cartwright JHE. Nonlinear stiffness, Lyapunov exponents, and attractor dimension. Phys Lett A 1999;264(4):298–302.
[31] Gottwald GA, Melbourne I. A new test for chaos in deterministic systems. Proc R Soc Lond Ser A Math Phys Eng Sci 2004;460(2042):603–11.
[32] Xin B, Li Y. 0-1 test for chaos in a fractional order financial system with investment incentive. Abstr Appl Anal 2013;2013.
[33] Xin B, Wu Z. Neimark–Sacker bifurcation analysis and 0–1 chaos test of an interactions model between industrial production and environmental quality in a closed area. Sustainability 2015;7(8):10191–209.
[34] Ott E, Grebogi C, Yorke JA and. Controlling chaos. Phys Rev Lett 2007;64(11):1196.
[35] Lynch S. Dynamical systems with applications using mathematica. Springer; 2007.